

Benchmarking calculations of excitation energies and transition properties with spectroscopic accuracy of highly charged ions used for the fusion plasma and astrophysical plasma

Chunyu Zhang(张春雨), Kai Wang(王凯), Ran Si(司然), Jinqing Li(李金晴), Changxian Song(宋昌仙), Sijie Wu(吴思捷), Bishuang Yan(严碧霜), and Chongyang Chen(陈重阳)
Citation: Chin. Phys. B, 2023, 32 (**11**): 113102. DOI: 10.1088/1674-1056/acef07
Journal homepage: http://cpb.iphy.ac.cn; http://iopscience.iop.org/cpb

What follows is a list of articles you may be interested in

Fully relativistic many-body perturbation energies, transition properties, and lifetimes of lithium-like iron Fe XXIV

Shuang Li(李双), Min Zhao(赵敏), Guo-Qing Liu(刘国庆), Chang-Bao Hu(胡昌宝), and Guo-Zhu Pan(潘国柱)
Chin. Phys. B, 2023, 32 (**10**): 103101. DOI: 10.1088/1674-1056/acef01

Ridge regression energy levels calculation of neutral ytterbium (Z = 70)

Yushu Yu(余雨姝), Chen Yang(杨晨), and Gang Jiang(蒋刚)
Chin. Phys. B, 2023, 32 (**3**): 033101. DOI: 10.1088/1674-1056/acac08

Energy levels and magnetic dipole transition parameters for the nitrogen isoelectronic sequence

Mu-Hong Hu(胡木宏), Nan Wang(王楠), Pin-Jun Ouyang(欧阳品均),Xin-Jie Feng(冯新杰), Yang Yang(杨扬), and Chen-Sheng Wu(武晨晟)
Chin. Phys. B, 2022, 31 (**9**): 093101. DOI: 10.1088/1674-1056/ac7a12

Energy levels and transition data of $3p^6 3d^8$ and $3p^5 3d^9$ configurations in Fe-like ions (Z = 57, 60, 62, 64, 65)

Bao-Ling Shi(施宝玲), Yi Qin(秦毅), Xiang-Fu Li(李向富), Bang-Lin Deng(邓邦林), Gang Jiang(蒋刚), and Xi-Long Dou(豆喜龙)
Chin. Phys. B, 2022, 31 (**5**): 053102. DOI: 10.1088/1674-1056/ac4480

Spectroscopy and scattering matrices with nitrogen atom: Rydberg states and optical oscillator strengths

Yuhao Zhu(朱宇豪), Rui Jin(金锐), Yong Wu(吴勇), and Jianguo Wang(王建国)
Chin. Phys. B, 2022, 31 (**4**): 043103. DOI: 10.1088/1674-1056/ac1f05

DATA PAPER

Benchmarking calculations of excitation energies and transition properties with spectroscopic accuracy of highly charged ions used for the fusion plasma and astrophysical plasma

Chunyu Zhang(张春雨)[1,2], Kai Wang(王凯)[3,4,†], Ran Si(司然)[1,‡], Jinqing Li(李金晴)[1], Changxian Song(宋昌仙)[1], Sijie Wu(吴思捷)[1], Bishuang Yan(严碧霜)[1], and Chongyang Chen(陈重阳)[1,§]

[1] *Shanghai EBIT Laboratory, Key Laboratory of Nuclear Physics and Ion-beam Application, Institute of Modern Physics, Department of Nuclear Science and Technology, Fudan University, Shanghai* 200433, *China*

[2] *Department of Physics, University of Strathclyde, Glasgow G*4 0*NG, UK*

[3] *Department of Physics and Anhui Key Laboratory of Optoelectric Materials Science and Technology, Key Laboratory of Functional Molecular Solids, Ministry of Education, Anhui Normal University, Wuhu* 241000, *China*

[4] *Hebei Key Laboratory of Optic-electronic Information and Materials, The College of Physics Science and Technology, Hebei University, Baoding* 071002, *China*

(Received 27 May 2023; revised manuscript received 23 July 2023; accepted manuscript online 11 August 2023)

Atomic radiative data such as excitation energies, transition wavelengths, radiative rates, and level lifetimes with high precision are the essential parameters for the abundance analysis, simulation, and diagnostics in fusion and astrophysical plasmas. In this work, we mainly focus on reviewing our two projects performed in the past decade. One is about the ions with $Z \lesssim 30$ that are generally of astrophysical interest, and the other one is about the highly charged krypton ($Z = 36$) and tungsten ($Z = 74$) ions that are relevant in research of magnetic confinement fusion. Two different and independent methods, namely, multiconfiguration Dirac–Hartree–Fock (MCDHF) and the relativistic many-body perturbation theory (RMBPT) are usually used in our studies. As a complement/extension to our previous works for highly charged tungsten ions with open M-shell and open N-shell, we also mainly focus on presenting and discussing our complete RMBPT and MCDHF calculations for the excitation energies, wavelengths, electric dipole (E1), magnetic dipole (M1), electric quadrupole (E2), and magnetic quadrupole (M2) transition properties, and level lifetimes for the lowest 148 levels belonging to the $3l^3$ configurations in Al-like W^{61+}. We also summarize the uncertainties of our systematical theoretical calculations, by cross-checking/validating our datasets from our RMBPT and MCDHF calculations, and by detailed comparisons with available accurate observations and other theoretical calculations. The data are openly available in Science Data Bank at https://doi.org/10.57760/sciencedb.10569.

Keywords: energy levels, transition rates, highly charged ions, relativistic many-body perturbation theory (RMBPT), multi-configuration Dirac–Hartree–Fock (MCDHF), benchmarking calculations, excitation energies, spectroscopic accuracy

PACS: 31.15.ag, 31.15.aj, 31.15.am **DOI:** 10.1088/1674-1056/acef07

1. Introduction

The ions with $Z \leq 30$, especially the ions of iron group elements, produce several strong transitions that have been widely used in astrophysics for a range of diagnostic applications, e.g., measuring electron temperatures, densities, chemical composition, and even strong magnetic fields,[1] for a review of some of the applications, see Del Zanna & Mason. Providing accurate atomic data for these ions is of paramount importance. In the tokamak fusion reactors, such as ITER[2] and EAST,[3,4] tungsten is an element proposed to be used as an erosion-resistant construction material. Therefore, highly-charged tungsten ions are of great interest in fusion plasma research.[5–9] The core temperature of ITER is projected to be of the order of 20 keV, possibly reaching as high as 30–40 keV under certain operating conditions.[10,11] At this temperature, highly-charged tungsten ions, with open *L*-shell, *M*-shell, or *N*-shell, have a large fractional abundance in the core plasma. The x-ray and extreme ultraviolet (EUV) spectra emitted from these tungsten ions, therefore, constitute the solid base of diagnostics for ITER plasma properties (such as temperature and density) and the bulk velocity of the plasma core.[8,12] Additionally, krypton is widely used as an injected impurity for diagnosing tokamak fusion plasmas,[13–17] and is also used as a diagnostic element for the x-ray imaging spectrometer system in the ITER.[18,19]

Atomic data such as excitation energies, transition wavelengths, radiative rates, and level lifetimes with high precision are necessary for plasma diagnostics and for interpreting the

†Corresponding author. E-mail: wang_kai10@fudan.edu.cn
‡Corresponding author. E-mail: rsi@fudan.edu.cn
§Corresponding author. E-mail: chychen@fudan.edu.cn

© 2023 Chinese Physical Society and IOP Publishing Ltd

plasma spectra. Experiments with their limited resources are unlikely to ever be able to provide complete datasets on any atomic systems. Instead, the bulk of the data must be provided by theoretical calculations. Based on fundamental principles and well-justified approximations, theoretical atomic physics derives and implements algorithms and computational procedures that yield the desired data.

The atomic spectroscopy group of Fudan University has mainly carried out two projects in collaboration with other groups in the past decade. One project focuses on the ions with $Z \lesssim 30$ that are generally of astrophysical interest, and the other one is about krypton ($Z = 36$) and tungsten ions ($Z = 74$) that are relevant in research of magnetic confinement fusion. Employing the multiconfiguration Dirac–Hartree–Fock (MCDHF) approach[20,21] implemented in the GRASP2K package,[22] and/or the relativistic many-body perturbation theory (RMBPT)[23–25] or relativistic configuration interaction (FAC-RCI)[26] implemented within the FAC package,[27,28] a large amount of atomic data including level energies, transition wavelengths, line strength, oscillator strengths, radiative rates and level lifetimes were obtained. By using the two different and independent methods (MCDHF and RMBPT), we cross-check/validate our two datasets and guarantee the self-consistency of our theoretical calculations. Additionally, by detailed comparisons with available accurate observations and theoretical calculations in the literature, we comprehensively assess the uncertainties of our calculations (see the summary in Section 4). The high accuracy of our systematic calculations makes them the preferable source of spectroscopic data for modelling plasma spectra and opens up new possibilities for their usage for the calibration of experimental x-ray and extreme ultraviolet (EUV) spectra.

The paper is organized as follows. The MCDHF and RMBPT methods are outlined in Section 2. In Subsection 3.1, we review the results from recent accurate RMBPT and MCDHF calculations for K-, L-, and M-shells ions with $Z \leq 42$. In Subsection 3.4, we review our previous works for tungsten ions with open M-shell and open N-shell, and present and discuss our complete RMBPT and MCDHF calculations for the excitation energies, electric dipole (E1), magnetic dipole (M1), electric quadrupole (E2), and magnetic quadrupole (M2) transition properties, and level lifetimes for the lowest 148 levels belonging to the $3l^3$ configurations in Al-like W^{61+}. The conclusions and outlook are shown in Section 4. If not explicitly indicated, atomic units are used throughout this work.

2. Outline of theory

2.1. MCDHF

The MCDHF method[20,21] implemented in the GRASP2K package[22] has been discussed in our recent studies.[29,30] Here, we only give a brief description. The MCDHF method starts from the Dirac–Coulomb (DC) Hamiltonian

$$H_{\rm DC} = \sum_{i=1}^{N} \left(c\, \boldsymbol{\alpha}_i \cdot \boldsymbol{p}_i + V_{\rm nuc}(r_i) + c^2(\beta_i - 1) \right) + \sum_{j>i=1}^{N} \frac{1}{r_{ij}}, \quad (1)$$

where $V_{\rm nuc}(r_i)$ is the nuclear potential, r_i is the electron–nucleus distance, r_{ij} is the distance between electrons i and j, c is the speed of light, N is the number of electrons, and $\boldsymbol{\alpha}_i$ and β_i denote the Dirac matrices.

Electron correlation is included by expanding the atomic state wave function (ASF) $\Psi(\Gamma J\pi)$ in a linear combination of configuration state functions (CSFs)

$$\Psi(\Gamma J\pi) = \sum_{i=1}^{M} c_i \Phi(\gamma_i J\pi), \quad (2)$$

where $\{\gamma_i\}$ specifies the occupied subshells with their complete angular coupling tree information of the CSFs, J and π are respectively the total angular momentum and the parity, and M is the number of CSFs. Each CSF, $\Phi(\gamma_i J\pi)$, is a jj-coupled many-electron function built from antisymmetrized products of one-electron Dirac orbitals.[20] The radial functions of the large and small components of the one-electron Dirac orbitals and the expansion coefficients $\{c_i\}$ of the CSFs are obtained by solving iteratively the relativistic self-consistent field (RSCF) radial equations for the orbitals, coupled to the matrix diagonalization for the targeted eigenvectors.

Once the orbitals have been optimized through the MCDHF procedure, the Breit interaction and higher-order (HO) retardation correction beyond the Breit interaction, as well as the leading quantum electrodynamic (QED) effects including self-energy (SE) and vacuum polarization (VP), are added to the Dirac–Coulomb Hamiltonian in the RCI calculations to capture relativistic corrections to the Coulomb interaction (see Refs. [29,30] for more details).

It should be noted that the SE correction is evaluated with a model QED operator developed recently by Shabaev *et al.*[31,32] It has been implemented in GRASP2K to study the ground-term fine structures of F-like[33] and Co-like ions,[34] and was also used in our recent benchmark works on W^{56+}–W^{61+}.[29,30] The SE correction is determined by evaluating the matrix element of the model self-energy operator

$$h^{\rm SE} = h^{\rm SE}_{\rm loc} + \sum_{i,j=1}^{n} |\phi_i\rangle \Big\{ \sum_{k,l=1}^{n} [(S^{\rm t})^{-1}]_{ik} \langle \psi_k |$$

$$\times\left\{\frac{1}{2}\left[\sum(\varepsilon_k)+\sum(\varepsilon_l)\right]-h_{\rm loc}^{\rm SE}\right\}|\psi_l\rangle(S^{-1})_{lj}\Big\}\langle\phi_j|, \quad (3)$$

with the many-electron wavefunction. In the latter equation, $h_{\rm loc}^{\rm SE}$ is a quasi-local operator acting differently on wavefunctions of different angular symmetry, $\{\phi_i(\boldsymbol{r})\}_{i=1}^{n}$ is the model basis of projected functions, $\{\psi_i(\boldsymbol{r})\}_{i=1}^{n}$ is the basis of the hydrogenic wavefunctions, and S_{ik} is the overlap matrix element $S_{ik}=\langle\phi_i|\psi_k\rangle$ (see the original work[31,32] for more details, including definitions of all quantities and ranges of summation).

2.2. RMBPT

The RMBPT method[23–25] is implemented in FAC.[27,28] This method is based on an approximation of the Dirac–Coulomb–Breit (DCB) Hamiltonian $H_{\rm DCB}=H_{\rm DC}+H_{\rm Breit}$. Then the $H_{\rm DCB}$ operator is split into a zeroth-order model Hamiltonian H_0 and a perturbation H', i.e., $H_{\rm DCB}=H_0+H'$, with[23,28]

$$H_0=\sum_i[h_{\rm D}(i)+U(r_i)], \quad (4)$$

$$H'=-\sum_i\left[\frac{Z}{r_i}+U(r_i)\right]+\sum_{i<j}\left(\frac{1}{r_{ij}}+B_{ij}\right), \quad (5)$$

where $h_{\rm D}(i)$ is the Dirac Hamiltonian for one free electron, Z is the nuclear charge, r_i is the radial coordinate of the electron i, and r_{ij} is the distance between the electrons i and j. B_{ij} is the frequency-independent Breit interaction. $U(r_i)$ is a one-electron model potential including the screening effects of all electrons, whose appropriate choice makes H' as small as possible. $U(r_i)$ is approximated by a local central potential and is derived from a Dirac–Fock–Slater self-consistent field calculation with the Hamiltonian H_0, which minimizes the weighted mean energy of all relevant configurations. After $U(r_i)$ is determined, the eigenfunctions Φ_k^0 and eigenvalues E_k^0 of H_0 can be calculated. The Φ_k^0 is divided into a model space M and the orthogonal space N. The effect of the states outside the M space is as usual taken into account by means of a perturbation expansion and expressed in terms of an "effective" Hamiltonian $H_{\rm eff}$ that operates only within the M space. $H_{\rm eff}$ is defined as

$$H_{\rm eff}=PH_0P+PH'\Omega, \quad (6)$$

where P is a projection operator that produces a state Ψ_k^0 in the M space when it operates on an eigenfunction Ψ_k of the full Hamiltonian, where Ψ_k^0 is a linear combination of the subset of Φ_k^0 that belongs to the M space. Ω is the wave operator that transforms Ψ_k^0 back to Ψ_k. The eigenvalues of $H_{\rm eff}$ are the true eigenenergies of the full Hamiltonian.

The matrix element of the first-order $H_{\rm eff}$ can be written as

$$\langle\Phi(\gamma_iJ\pi)|H_{\rm eff}^{(1)}|\Phi(\gamma_jJ\pi)\rangle=(H_{\rm DCB})_{ij}+\sum_{r\in N}\frac{H'_{ir}H'_{rj}}{E_j^0-E_r^0}, \quad (7)$$

where $(H_{\rm DCB})_{ij}=\langle\Phi(\gamma_iJ\pi)|H_{\rm DCB}|\Phi(\gamma_jJ\pi)\rangle$ and $H'_{ir}=\langle\Phi(\gamma_iJ\pi)|H'|\Phi(\gamma_rJ\pi)\rangle$ $(i,j\in M, r\in N)$. By solving the generalized eigenvalue problem for the first-order $H_{\rm eff}$, we can obtain the eigenvalues in the second-order approximation.

The Breit interaction, the higher-order retardation correction beyond the Breit interaction, and the leading QED corrections are also considered in the same way as for the MCDHF calculations.

2.3. Transition properties

Transition properties such as line strengths S, weighted oscillator strengths gf, and radiative rates A from the state γPJ to the state $\gamma'P'J'$ are computed in perturbation theory in terms of reduced matrix elements

$$\langle\Psi(\gamma PJ)\|\boldsymbol{T}^{(\rm EMK)}\|\Psi(\gamma'P'J')\rangle, \quad (8)$$

where the operator $\boldsymbol{T}^{(\rm EMK)}$ depends on the multipolarity (E1, M1, E2, M2, etc.) of the transition. Inserting the CSF expansions for the wave functions, the reduced matrix element reduces to a sum over reduced matrix elements between CSFs. These matrix elements are finally obtained as sums over radial integrals using Racah algebra techniques. The above procedure assumes that the two states γPJ and $\gamma'P'J'$ are built from the same set of orbitals. When this is not the case, e.g., when separate calculations have been done for the even and odd parity states, the representations of the wave functions are changed in such a way that the orbitals become biorthonormal,[35] in which case the calculation continues along the lines above. For electric transitions, the parameters can be computed in both length and velocity gauges,[36] where the results in the length gauge are preferred.

3. Results and discussion

3.1. *K*-, *L*-, and *M*-shells ions with $Z\leq 42$

Using at least one of the three methods (RMBPT, MCDHF, and FAC-RCI), we carried out many theoretical studies of excitation energies and E1, M1, E2, M2 transition rates for K- and L-shell ions with $Z\leq 42$, such as the ions in the sequences of H-like,[37,38] He-like,[39,40] Be-like,[41–45] B-like,[46–48] C-like,[49,50] N-like,[51–55] O-like,[56–60] F-like,[61–63] and Ne-like.[64] It is important to provide atomic data for more than just the levels of the lowest configurations in plasma modeling and diagnostics. To meet the demand for data, calculations of different ions in the He-, Be-, B-, C-, N-, O-, F-, and Ne-like sequences were provided from several dozen levels to several hundred levels, which are referred to as spectrum calculations. The range of ions, the targeted configurations and the number of studied states for each sequence are summarized in Table 1.

Table 1. Sequence, atomic number (Z) of ions, targeted configurations, methods of the calculations, and the number (N) of studied states for each ion. In the table, $l = 0,\ldots,n-1$ and $l' = 0,\ldots,n'-1$. The excitation energies, E1, M1, E2, M2, E3, and M3 transition properties are studied for the targeted states in our previous works listed in the last column.

Sequence	Z	Configurations	Methods	N	Refs.
H-like	13–42	nl ($n \le 6$)	FAC-RCI	36	[37,38]
He-like	10–36	$1snl$ ($n \le 6$), $2l'nl$ ($l' \le 2$, $n \le 6$)	RMBPT&MCDHF	321	[39,40]
Be-like	5–7	$2snl$ ($n \le 6$), $2pnl$ ($n \le 6$)	MCDHF	100	[41]
	8–10	$2snl$ ($n \le 6$), $2pnl$ ($n \le 6$)	MCDHF	138	[41]
	11–30	$2snl$ ($n \le 5$), $2pnl$ ($n \le 4$)	RMBPT	116	[42]
	32, 36	$2snl$ ($n \le 4$), $2pnl$ ($n \le 4$)	RMBPT&MCDHF	98	[43]
	39	$2snl$ ($n \le 5$), $2pnl$ ($n \le 5$)	RMBPT	166	[44]
	42	$2snl$ ($n \le 6$), $2pnl$ ($n \le 6$)	RMBPT&MCDHF	250	[45]
B-like	16	$2s^2nl$ ($n \le 5$), $2s2pnl$ ($n \le 4$), $2p^2nl$ ($n \le 3$)	RMBPT&MCDHF	213	[46]
	24–30	$2s^2nl$ ($n \le 5$), $2s2pnl$ ($n \le 5$), $2p^2nl$ ($n \le 5$)	RMBPT&MCDHF	513	[47]
	36	$2s^2nl$ ($n \le 5$), $2s2pnl$ ($n \le 5$), $2p^2nl$ ($n \le 5$)	RMBPT&MCDHF	513	[48]
C-like	8	$2s^22pnl$ ($n \le 5$), $2s2p^2nl$ ($n \le 4$), $2p^2nl$ ($n \le 3$)	MCDHF	156	[49]
	9	$2s^22pnl$ ($n \le 5$), $2s2p^2nl$ ($n \le 4$), $2p^2nl$ ($n \le 3$)	MCDHF	196	[49]
	10	$2s^22pnl$ ($n \le 5$), $2s2p^2nl$ ($n \le 4$), $2p^2nl$ ($n \le 3$)	MCDHF	215	[49]
	11	$2s^22pnl$ ($n \le 5$), $2s2p^2nl$ ($n \le 4$), $2p^2nl$ ($n \le 3$)	MCDHF	272	[49]
	12	$2s^22pnl$ ($n \le 5$), $2s2p^2nl$ ($n \le 4$), $2p^2nl$ ($n \le 3$)	MCDHF	318	[49]
	13–36	$2s^22pnl$ ($n \le 3$), $2s2p^2nl$ ($n \le 3$), $2p^2nl$ ($n \le 3$)	RMBPT	46	[50]
N-like	18–30	$2s^22p^2nl$ ($n \le 4$), $2s2p^3nl$ ($n \le 3$), $2p^4nl$ ($n \le 3$)	RMBPT	359	[51]
	32	$2s^22p^2nl$ ($n \le 3$), $2s2p^3nl$ ($n \le 3$), $2p^4nl$ ($n \le 3$)	RMBPT&MCDHF	272	[52]
	34	$2s^22p^2nl$ ($n \le 4$), $2s2p^3nl$ ($n \le 3$), $2p^4nl$ ($n \le 3$)	RMBPT&MCDHF	316	[53]
	36	$2s^22p^2nl$ ($n \le 3$), $2s2p^3nl$ ($n \le 3$), $2p^4nl$ ($n \le 3$)	RMBPT&MCDHF	272	[54]
	40	$2s^22p^2nl$ ($n \le 3$), $2s2p^3nl$ ($n \le 3$), $2p^4nl$ ($n \le 3$)	RMBPT&MCDHF	272	[55]
O-like	18	$2s^22p^3nl$ ($n \le 3$), $2s2p^4nl$ ($n \le 3$), $2p^6$	MCDHF	156	[56]
	19	$2s^22p^3nl$ ($n \le 3$), $2s2p^4nl$ ($n \le 3$), $2p^6$	MCDHF	179	[56]
	20	$2s^22p^3nl$ ($n \le 3$), $2s2p^4nl$ ($n \le 3$), $2p^6$	MCDHF	196	[56]
	21–23	$2s^22p^3nl$ ($n \le 3$), $2s2p^4nl$ ($n \le 3$), $2p^6$	MCDHF	200	[56]
	24–30	$2s^22p^3nl$ ($n \le 3$), $2s2p^4nl$ ($n \le 3$), $2p^6$	RMBPT&MCDHF	200	[57]
	34	$2s^22p^3nl$ ($n \le 4$), $2s2p^4nl$ ($n \le 3$), $2p^5nl$ ($n \le 3$)	RMBPT&MCDHF	318	[58]
	36	$2s^22p^3nl$ ($n \le 4$), $2s2p^4nl$ ($n \le 4$), $2p^5nl$ ($n \le 3$)	RMBPT&MCDHF	344	[59]
	42	$2s^22p^3nl$ ($n \le 4$), $2s2p^4nl$ ($n \le 3$), $2p^5nl$ ($n \le 3$)	RMBPT&MCDHF	318	[60]
F-like	24–30	$2s^22p^4nl$ ($n \le 4$), $2s2p^5nl$ ($n \le 3$), $2p^6nl$ ($n \le 3$)	RMBPT&MCDHF	200	[61]
	31–35	$2s^22p^4nl$ ($n \le 4$), $2s2p^5nl$ ($n \le 3$), $2p^6nl$ ($n \le 3$)	RMBPT&MCDHF	200	[62]
	36	$2s^22p^4nl$ ($n \le 4$), $2s2p^5nl$ ($n \le 3$), $2p^6nl$ ($n \le 3$)	RMBPT&MCDHF	200	[63]
Ne-like	24–36	$2s^22p^5nl$ ($n \le 6$), $2s2p^6nl$ ($n \le 4$)	RMBPT	201	[64]

3.1.1. Excitation energies

The accuracy of all atomic structure calculations, including RMBPT and MCDHF, is determined by the way of comparing theoretical and experimental results, or by the way of comparing between accurate theoretical results of different calculations. Generally speaking, a trend for all atomic structure calculations, including RMBPT and MCDHF, is that the accuracy of excitation energies increases as the atomic number Z increases and the effect of electron correlation diminishes along the isoelectronic sequence.

For example, in the study of O-like ions,[57] a comparison between the MCDHF and RMBPT excitation energies is carried out along the sequence with $Z = 24$–30. Defining $\Delta E_i \equiv (E^i_{\rm RMBPT} - E^i_{\rm MCDHF})$ for each of the N energy levels that can be compared ($i = 1,\ldots,N$, and $N = 200$), the average absolute difference between the two sets calculated from

$$\overline{\Delta E} = \frac{\sum_{i=1}^{N} \Delta E_i}{N}, \tag{9}$$

with the standard deviation

$$\sigma_1 = \sqrt{\frac{\sum_{i=1}^{N} (\Delta E_i - \overline{\Delta E})^2}{(N-1)}}, \tag{10}$$

decreases from -623 ± 606 cm^{-1} for Cr XVII to -397 ± 536 cm^{-1} for Zn XXIII. These correspond to average relative differences $(\overline{\Delta x} \pm \sigma_2)$ from $-0.012\% \pm 0.021\%$ for Cr XVII to $-0.009\% \pm 0.016\%$ for Zn XXIII, with

$$\overline{\Delta x} \equiv \frac{\sum_{i=1}^{N} \Delta x_i}{N} = \frac{\sum_{i=1}^{N} (E^i_{\rm RMBPT}/E^i_{\rm MCDHF} - 1)}{N}, \tag{11}$$

$$\sigma_2 = \sqrt{\frac{\sum_{i=1}^{N} (\Delta x_i - \overline{\Delta x})^2}{(N-1)}}. \tag{12}$$

In the study of F-like ions with $Z = 24$–30,[61] the same trend is found as the atomic number Z increases along the isoelectronic sequence. The average relative differences

($\overline{\Delta x} \pm \sigma_2$) also decrease from 0.003%±0.016% for Cr XVI to 0.002%±0.007% for Zn XXII.

In Table 2 excitation energies in O-like Ni XXI from different calculations are compared with experimental values from the Atomic Spectra Database (ASD) of the National Institute of Standards and Technology (NIST).[65] Our MCDHF and RMBPT excitation energies are in good agreement, with the average absolute difference of $\overline{\Delta E} \pm \sigma_1 = -481 \pm 511$ cm^{-1}. The previous theoretical energies from Refs. [66–68] depart from our MCDHF values with average difference of $1\,379 \pm 14\,851$ cm^{-1}, $29\,279 \pm 15\,742$ cm^{-1}, and $634 \pm 24\,996$ cm^{-1}, respectively. Compared with the previous calculations, the average difference/uncertainty of the present MCDHF and RMBPT calculations go down by one or two orders of magnitude, and now, the calculated energies are accurate enough to detect misidentifications or errors in observational data, but also to serve as a valuable tool for identifying new lines.

Though many of the NIST excitation energies of Ni XXI show good agreement with our MCDHF and RMBPT values, the deviations from our values are larger than 10 000 cm^{-1} for a few levels. For example, experimental energies from the NIST ASD are questionable for a few $n = 3$ states of Ni XXI. The values 8 035 000 cm^{-1} for #12/$2s^2 2p^3(^4S)3s\ ^3S_1$, 8 313 000 cm^{-1} for #22/$2s^2 2p^3(^2P)3s\ ^3P_1$, 8 405 000 cm^{-1} for #26/$2s^2 2p^3(^2P)3s\ ^3P_2$, and 8 422 000 cm^{-1} for #26/$2s^2 2p^3(^2P)3s\ ^1P_1$ do not have obvious counterparts in the present MCDHF and RMBPT calculations. Another 6 NIST values for the $2s^2 2p^3 3d$ levels, shown in Table 2, also deviate from our values by greater than 10 000 cm^{-1}.

Table 2. Energy levels (in cm^{-1}) relative to the ground state for the lowest 200 states of Ni XXI. For brevity, energies other than the present MCDHF values are listed as differences from the latter ones in cm^{-1}. $E_{\rm MCDHF}$, $E_{\rm RMBPT}$ – the present calculations; $E_{\rm NIST}$;[65] $E_{\rm Fan}$:[66] $E_{\rm Bhatia}$:[67] $E_{\rm Aggarwal}$.[68] Our RMBPT and MCDHF results shown in this table are published in their entirety online.

Key	Configuration	Term	$E_{\rm MCDHF}$	$E_{\rm RMBPT}$	$E_{\rm NIST}$	$E_{\rm Fan}$	$E_{\rm Bhatia}$	$E_{\rm Aggarwal}$
1	$2s^2 2p^4$	$^3P_2$	0	0	0	0	0	0
2	$2s^2 2p^4$	$^3P_0$	92923	–104	–102	–1226	–1364	29
3	$2s^2 2p^4$	$^3P_1$	128291	133	–1	–859	712	–838
4	$2s^2 2p^4$	$^1D_2$	212368	–57	–118	1621	3578	1698
5	$2s^2 2p^4$	$^1S_0$	406998	–126	–198	–3435	–1953	–77
6	$2s2p^5$	$^3P_2$	1043158	–472	–8	17533	5222	12414
7	$2s2p^5$	$^3P_1$	1125915	–433	–65	17880	5718	12675
8	$2s2p^5$	$^3P_0$	1193024	–376	–64	16489	5868	11771
9	$2s2p^5$	$^1P_1$	1436593	–567	–193	31702	16635	21893
10	$2p^6$	$^1S_0$	2403767	–1469	–267	66386	41807	40226
12	$2s^2 2p^3(^4S)3s$	$^3S_1$	8024448	–242	10552	–6429	30355	–8774
13	$2s^2 2p^3(^2D)3s$	$^3D_2$	8146451	–30	–451	–3890	31132	–7344
14	$2s^2 2p^3(^2D)3s$	$^3D_1$	8152417	–116	–6417	–5690	29220	–7132
15	$2s^2 2p^3(^2D)3s$	$^3D_3$	8193361	–110	–2361	–7784	26819	–6354
16	$2s^2 2p^3(^2D)3s$	$^1D_2$	8214215	–191	–2215	–7430	27236	–5655
20	$2s^2 2p^3(^2P)3s$	$^3P_0$	8288106	33	6894	16074	47630	–2291
22	$2s^2 2p^3(^2P)3s$	$^3P_1$	8296828	66	16172	15813	47412	–10048
26	$2s^2 2p^3(^2P)3s$	$^3P_2$	8386599	86	18401	10849	39844	–9351
27	$2s^2 2p^3(^2P)3s$	$^1P_1$	8402772	–52	19228	11773	40706	1669
51	$2s^2 2p^3(^4S)3d$	$^3D_3$	8668854	–789	–2854	–6608	33461	–3831
68	$2s^2 2p^3(^2D)3d$	$^3D_3$	8840222	–811	–5222	–3935	33573	30
71	$2s^2 2p^3(^2D)3d$	$^3D_2$	8850798	–723	–2798	–3653	33832	–5696
75	$2s^2 2p^3(^2D)3d$	$^1F_3$	8898236	–985	–2236	–1190	34633	1065
78	$2s^2 2p^3(^2P)3d$	$^3F_3$	8928972	–445	–33972			–6088
79	$2s^2 2p^3(^2P)3d$	$^1D_2$	8941104	–603	106896	–272	36340	–2879
85	$2s^2 2p^3(^2P)3d$	$^3P_2$	9010165	–335	–86165	–55761	–20486	–5977
86	$2s^2 2p^3(^2P)3d$	$^3P_1$	9014227	–440	–14227	12092	45525	–5013
89	$2s^2 2p^3(^2P)3d$	$^1F_3$	9051790	–980	–3790	14294	45911	–327
91	$2s^2 2p^3(^2P)3d$	$^3D_2$	9058604	–695	–24604	–38601	–4235	–2071
94	$2s^2 2p^3(^2P)3d$	$^1P_1$	9123093	–994	–33093	18511	46504	950

For many L-shell ions with $Z \leq 42$, excitation energies for lower-lying states are known from observations. Going higher up comparatively less data are available, often associated with large uncertainties. The excellent description of energy separations of our calculations (MCDHF and/or RMBPT) along the isoelectronic sequence makes it possible to point out a number of lines for which experimental identifications are questionable. As an example, in Fig. 1(a) we show the deviations of experimental values from the NIST ASD to our MCDHF excitation energies as a function of Z for

the $2s^22p^3(^4S)3s\ ^3S_1$, $2s^22p^3(^2P)3s\ ^1P_1$, $2s^22p^3(^4S)3d\ ^3D_3$, and $2s^22p^3(^2D)3d\ ^3D_3$ levels of O-like ions. The deviations between the RMBPT and MCDHF excitation energies for the same levels along the sequence are shown in Fig. 1(b). Good agreement is obtained between the present MCDHF and RMBPT values for the same levels along the sequence, and the differences between the two data sets (MCDHF and RMBPT) vary smoothly along the isoelectronic sequence. In comparison, a few of the NIST values depart from the MCDHF excitation energies by over 10 000 cm^{-1}. Therefore, these experimental values compiled by the NIST ASD seem to be wrong or at least are affected by large errors. The situation is also well illustrated for the ions in the other L-shell sequences of Be-like,[41,42] B-like,[46,47] C-like,[49,50] N-like,[51] F-like,[61,62] and Ne-like.[64]

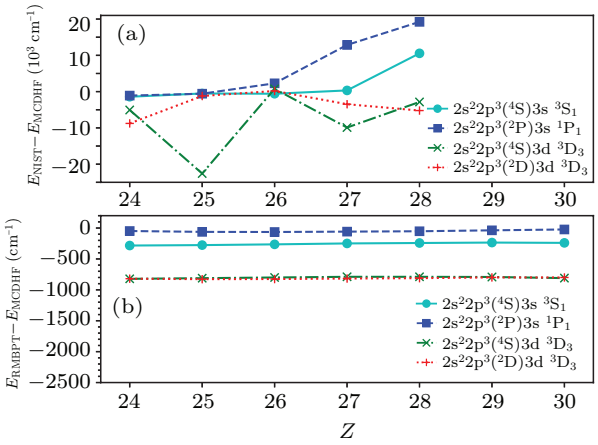


Fig. 1. Energy deviations ((a) $E_{NIST} - E_{MCDHF}$ and (b) $E_{RMBPT} - E_{MCDHF}$) in cm^{-1} as a function of Z for the $2s^22p^3(^4S)3s\ ^3S_1$, $2s^22p^3(^2P)3s\ ^1P_1$, $2s^22p^3(^4S)3d\ ^3D_3$, and $2s^22p^3(^2D)3d\ ^3D_3$ levels of O-like ions.

The M-shell ions with $Z \leq 30$, especially the ions of iron group elements, produce strong extreme ultraviolet (EUV) spectral lines, which are routinely used to measure electron densities using data from, e.g., the SOHO Coronal Diagnostic Spectrometer (CDS), see Ref. [69] and especially the Hinode EUV Imaging Spectrometer (EIS), see Refs. [70–74]. The soft x-ray spectra are also rich in $n = 4 \rightarrow n = 3$ transitions from M-shells ions of iron group elements.[75–77] Various current missions, such as Chandra with the Low Energy Transmission Grating (LETG), and the Solar Dynamic Observatory (SDO) with a suite of instruments, cover this wavelength range.[78,79]

Using the MCDHF method, we carried out many theoretical studies of excitation energies and E1, M1, E2, and M2 transition rates for M-shell ions with $Z \leq 32$, such as the ions in the sequences of Si-like,[80] P-like,[81,82,85] S-like,[83] and Cl-like.[84] The range of ions in different isoelectronic sequences, the targeted configurations, and the number of studied states for each ion of each sequence are summarized in Table 3.

Table 3. Sequence, atomic number (Z) of ions, targeted configurations, and methods of the calculations, the number (N) of studied states for each ion. In the table $l = 0, \ldots, n-1$, and $l' = 0, \ldots, n'-1$. The excitation energies, E1, M1, E2, and M2 transition properties are studied for the targeted states in our previous works listed in the last column.

Sequence	Z	Configurations	Methods	N	Refs.
Si-like	24	$3l^4, 3l^34l', 3l^35l'$	MCDHF	604	[80]
	25	$3l^4, 3l^34l', 3l^35l'$	MCDHF	699	[80]
	26	$3l^4, 3l^34l', 3l^35l'$	MCDHF	702	[80]
	27–29	$3l^4, 3l^34l', 3l^35l'$	MCDHF	704	[80]
	30	$3l^4, 3l^34l', 3l^35l'$	MCDHF	699	[80]
P-like	25	$3l^5, 3l^44l'$	MCDHF	546	[81]
	26	$3l^5, 3l^44l'$	MCDHF	623	[81]
	27	$3l^5, 3l^44l'$	MCDHF	701	[81]
	28	$3l^5, 3l^44l'$	MCDHF	745	[81]
	32	$3l^5$	MCDHF	150	[82]
S-like	24	$3l^6$	MCDHF	159	[83]
	25	$3l^6$	MCDHF	227	[83]
	26	$3l^6$	MCDHF	236	[83]
	27	$3l^6$	MCDHF	304	[83]
	28	$3l^6$	MCDHF	376	[83]
	29	$3l^6$	MCDHF	436	[83]
Cl-like	24	$3l^7$	MCDHF	187	[84]
	25	$3l^7$	MCDHF	196	[84]
	26	$3l^7$	MCDHF	197	[84]
	27	$3l^7$	MCDHF	193	[84]
	28	$3l^7$	MCDHF	192	[84]
	29–30	$3l^7$	MCDHF	194	[84]

We reviewed the identifications of the transitions $n = 4 \rightarrow 3$ and $n = 3 \rightarrow 3$ of Fe XIII, Fe XII, Fe XI, and Fe X, and some new identifications for these four ions were proposed. As an example, the identifications of the transitions $n = 4 \rightarrow 3$ and $n = 3 \rightarrow 3$ of Fe XIII and Fe XII are shown in Table 4. Based on our MCDHF atomic data (wavelengths, radiative rates), and electron impact excitation rates provided by Del Zanna,[86,87] the relative intensities $\text{Int} = N_j A_{ji}/N_e$ (in photon units) are calculated using the collisional radiative model (CRM)[88] at a fixed temperature T_e [K] $= 10^{6.3}$ and at electron densities of 10^9 cm^{-3} (the first part) and 10^{13} cm^{-3} (the second part) relative to $3s\,3p^3\ ^3D^\circ_1 - 3s\,3p^2(^3P)\,4s\ ^3P_0$ (7–332) for Fe XIII, and 10^{19} cm^{-3}(the third part) for Fe XII relative to $3s^2\,3p^3(^4_3S)\ ^4S^\circ_{3/2} - 3s^2\,3p^2(^3_2P)\ ^3P4s\ ^4P_{5/2}$(1–292). The previous line identifications $n = 4 \rightarrow 3$ and $n = 3 \rightarrow 3$ of Fe XIII and Fe XII in the EUV and x-ray wavelength range are reviewed by comprehensively comparing the MCDHF values with available experimental data. Discrepancies in the previous identifications for several cases, i.e., 12 cases in Fe XIII and 8 cases in Fe XII, have been found, and some tentative new (or revised) identifications (19 lines in Fe XIII and 5 lines in Fe XII) have been proposed.

Table 4. A list of the strongest Fe XIII and Fe XII lines from the transition arrays $n = 3 \rightarrow n = 3$ and $n = 4 \rightarrow n = 3$. Using atomic data provided by Del Zanna,[86,87] the transitions are ordered by their relative intensities Int= $N_j A_{ji}/N_e$ (column 3, in photon units), calculated at electron densities of 10^9 cm^{-3} (the first part) and 10^{13} cm^{-3} (the second part) relative to $3s\,3p^3\ {}^3D^o_1$–$3s\,3p^2({}^3P)\,4s\ {}^3P_0$ (7–332) for Fe XIII, and 10^{19} cm^{-3} (the third part) for Fe XII relative to $3s^2\,3p^3({}^4_3S)\ {}^4S^o_{3/2}$–$3s^2\,3p^2({}^3_2P)\ {}^3P4s\ {}^4P_{5/2}$(1–292) . Column 4 gives the experimental wavelength λ_{exp} (Å) from CHIANTI or NIST. We add a 'No' if we consider the previous identification incorrect. Column 5 gives the AUTOSTRUCTURE (AS) wavelength λ_{AS} from Refs. [86,87]. Column 6 is our present wavelength λ_{MCDHF} (with a difference with the experimental one in bracket), while the following column (λ_{rev}) reports any new experimental wavelength that we propose. The last column indicates if the identification of a line is questionable (?) or new (N). D indicates a new identification proposed by Del Zanna.[73,86] Be72, MH73, FP, M72, D12, Be76, TN94: wavelengths from Refs. [76,77,89–93]. Some new wavelengths have been obtained from the spectra (the MH73 and FP spectra were reprocessed as described in Ref. [86]). More detailed information on Fe XIII and Fe XII line identifications can be found in our recent papers.[80,81]

Ions	i–j	Transition	Int	λ_{exp}	λ_{AS}	λ_{MCDHF}	λ_{rev}	Notes
			electron density (10^9 cm^{-3})					
Fe XIII	7–60	$3s\,3p^3\ {}^3D^o_1 - 3s\,3p^2({}^3P)\,3d\ {}^3F_2$	2.2	203.772^D	197.71	201.474 (2.298)	201.49	N (D12)
Fe XIII	9–28	$3s\,3p^3\ {}^3D^o_3 - 3p^4\ {}^3P_2$	1.9	332.025^D	319.01	319.956 (12.069)		?
Fe XIII	9–65	$3s\,3p^3\ {}^3D^o_3 - 3s\,3p^2({}^3P)\,3d\ {}^3F_4$	1.8	199.233^D	193.47	196.995 (2.238)	197.02	N (D12)
Fe XIII	8–61	$3s\,3p^3\ {}^3D^o_2 - 3s\,3p^2({}^3P)\,3d\ {}^3F_3$	1.5	201.538^D	195.62	199.210 (2.328)	199.24	N (D12)
Fe XIII	15–42	$3s^2\,3p\,3d\ {}^3F^o_2 - 3s\,3p^2({}^1D)\,3d\ {}^3F_2$	1.4	417.641^D	405.20	400.520 (17.12)	400.67	N (TN94)
Fe XIII	8–60	$3s\,3p^3\ {}^3D^o_2 - 3s\,3p^2({}^3P)\,3d\ {}^3F_2$	1.3	203.835^D	197.78	201.534 (2.301)	201.55	N (D12)
Fe XIII	2–17	$3s^2\,3p^2\ {}^3P_1 - 3s\,3p^3\ {}^1P^o_1$	1.2	233.218	229.66	232.984 (0.234)		?
Fe XIII	5–17	$3s^2\,3p^2\ {}^1S_0 - 3s\,3p^3\ {}^1P^o_1$	1.1	288.538	285.49	288.380 (0.158)		?
Fe XIII	8–56	$3s\,3p^3\ {}^3D^o_2 - 3s\,3p^2({}^3P)\,3d\ {}^3D_2$	1	214.403^D	208.02	211.212 (3.191)	211.20	N (D12)
Fe XIII	9–57	$3s\,3p^3\ {}^3D^o_3 - 3s\,3p^2({}^1D)\,3d\ {}^3D_3$	1	–	208.75	212.103		?
Fe XIII	14–84	$3s\,3p^3\ {}^3S^o_1 - 3s\,3p^2({}^3P)\,3d\ {}^3P_2$	0.84	207.448^D	203.77	207.637 (–0.189)	207.75	N (D12)
Fe XIII	12–67	$3s\,3p^3\ {}^3P^o_2 - 3s\,3p^2({}^3P)\,3d\ {}^3D_3$	0.78	–	209.00	212.451	212.32	N (D12)
Fe XIII	11–63	$3s\,3p^3\ {}^3P^o_1 - 3s\,3p^2({}^1D)\,3d\ {}^3D_2$	0.75	–	211.30	214.838		?
Fe XIII	16–72	$3s^2\,3p\,3d\ {}^3F^o_3 - 3s\,3p^2({}^1S)\,3d\ {}^3D_2$	0.7	262.984^D	256.74	260.001 (2.983)	259.963	N (Be76)
Fe XIII	7–332	$3s\,3p^3\ {}^3D^o_1 - 3s\,3p^2({}^3P)\,4s\ {}^3P_0$	1	76.507^D	75.71	76.852 (-0.345)	76.867	N (Be72)
Fe XIII	9–341	$3s\,3p^3\ {}^3D^o_3 - 3s\,3p^2({}^3P)\,4s\ {}^3P_2$	0.66	–	75.10	76.145	76.113	N (Be72)
Fe XIII	8–334	$3s\,3p^3\ {}^3D^o_2 - 3s\,3p^2({}^3P)\,4s\ {}^3P_1$	0.62	–	75.42	76.507	76.507	N (Be72)
Fe XIII	9–270	$3s\,3p^3\ {}^3D^o_3 - 3s^2\,3p4p\ {}^3P_2$	0.47	–	83.51	84.674	84.62	N (MH73)
Fe XIII	16–259	$3s^2\,3p\,3d\ {}^3F^o_3 - 3s^2\,3p4p\ {}^3D_2$	0.37	–	97.82	98.496	98.517	N (Be72)
Fe XIII	24–270	$3s^2\,3p\,3d\ {}^3D^o_3 - 3s^2\,3p4p\ {}^3P_2$	0.35	–	103.23	103.916	103.93	N (Be72)
Fe XIII	18–268	$3s^2\,3p\,3d\ {}^3F^o_4 - 3s^2\,3p4p\ {}^3D_3$	0.28	–	97.54	98.106	98.15	N (FP)
Fe XIII	12–341	$3s\,3p^3\ {}^3P^o_2 - 3s\,3p^2({}^3P)\,4s\ {}^3P_2$	0.27	–	77.51	78.548	78.56	N (M72)
			electron density (10^{13} cm^{-3})					
Fe XIII	9–341	$3s\,3p^3\ {}^3D^o_3 - 3s\,3p^2({}^3P)\,4s\ {}^3P_2$	3.3	–	75.1	76.145	76.113	N (Be72)
Fe XIII	9–270	$3s\,3p^3\ {}^3D^o_3 - 3s^2\,3p4p\ {}^3P_2$	2.3	–	83.51	84.674	84.62	N (MH73)
Fe XIII	8–334	$3s\,3p^3\ {}^3D^o_2 - 3s\,3p^2({}^3P)\,4s\ {}^3P_1$	2.1	–	75.42	76.507	76.507	N (Be72)
Fe XIII	18–268	$3s^2\,3p\,3d\ {}^3F^o_4 - 3s^2\,3p4p\ {}^3D_3$	1.8	–	97.54	98.106	98.128	N (FP)
Fe XIII	24–270	$3s^2\,3p\,3d\ {}^3D^o_3 - 3s^2\,3p4p\ {}^3P_2$	1.7	–	103.23	103.916	103.93	N (Be72)
Fe XIII	24–418	$3s^2\,3p\,3d\ {}^3D^o_3 - 3s^2\,3p4f\ {}^3F_4$	1.4	–	81.92	82.501	82.50	N (FP)
Fe XIII	12–341	$3s\,3p^3\ {}^3P^o_2 - 3s\,3p^2({}^3P)\,4s\ {}^3P_2$	1.3	–	77.51	78.548	78.56	N (FP)
Fe XIII	16–259	$3s^2\,3p\,3d\ {}^3F^o_3 - 3s^2\,3p4p\ {}^3D_2$	1.2	–	97.82	98.496	98.523	N (FP)
Fe XIII	7–332	$3s\,3p^3\ {}^3D^o_1 - 3s\,3p^2({}^3P)\,4s\ {}^3P_0$	1	76.507^D	75.71	76.852 (-0.345)	76.867	N (Be72)
Fe XIII	3–359	$3s^2\,3p^2\ {}^3P_2 - 3s^2\,3p4d\ {}^3P^o_2$	0.85	–	61.52	62.072	62.09	N (FP)
			electron density (10^{19} cm^{-3})					
Fe XIV	3–507	$3s^2\,3p^3({}^2_3D)\ {}^2D^o_{5/2} - 3s^2\,3p^2({}^3_2P)\ {}^3P4d\ {}^2F_{7/2}$	0.89	67.702 No	66.68	67.551 (–0.15)		?
Fe XIV	2–498	$3s^2\,3p^3({}^2_3D)\ {}^2D^o_{3/2} - 3s^2\,3p^2({}^3_2P)\ {}^3P4d\ {}^2F_{5/2}$	0.81	67.821 No	66.81	67.706	67.702	N (FP)
Fe XIV	1–488	$3s^2\,3p^3({}^4_3S)\ {}^4S^o_{3/2} - 3s^2\,3p^2({}^3_2P)\ {}^3P4d\ {}^4P_{5/2}$	0.75	66.297	65.31	66.324		?
Fe XIV	5–552	$3s^2\,3p^3({}^2_1P)\ {}^2P^o_{3/2} - 3s^2\,3p^2({}^1_2D)\ {}^1D4d\ {}^2D_{5/2}$	0.72	67.972 No	66.88	67.822 (–0.15)	67.821	N (FP)
Fe XIV	3 –497	$3s^2\,3p^3({}^2_3D)\ {}^2D^o_{5/2} - 3s^2\,3p^2({}^3_2P)\ {}^3P4d\ {}^4F_{7/2}$	0.57	–	67.11	67.975	67.972	N (FP)
Fe XIV	3–545	$3s^2\,3p^3({}^2_3D)\ {}^2D^o_{5/2} - 3s^2\,3p^2({}^1_2D)\ {}^1D4d\ {}^2F_{5/2}$	0.46	66.431	65.57	66.486		?
Fe XIV	3–561	$3s^2\,3p^3({}^2_3D)\ {}^2D^o_{5/2} - 3s^2\,3p^2({}^1_2D)\ {}^1D4d\ {}^2G_{7/2}$	0.41	–	65.06	65.999		?
Fe XIV	5–613	$3s^2\,3p^3({}^2_1P)\ {}^2P^o_{3/2} - 3s^2\,3p^2({}^1_0S)\ {}^1S4d\ {}^2D_{5/2}$	0.38	–	64.41	65.632		?
Fe XIV	2–548	$3s^2\,3p^3({}^2_3D)\ {}^2D^o_{3/2} - 3s^2\,3p^2({}^1_2D)\ {}^1D4d\ {}^2D_{3/2}$	0.33	–	65.30	66.235	66.224	? (FP)
Fe XIV	2–545	$3s^2\,3p^3({}^2_3D)\ {}^2D^o_{3/2} - 3s^2\,3p^2({}^1_2D)\ {}^1D4d\ {}^2F_{5/2}$	0.31	66.232 No	65.38	66.288	66.297	N (FP)
Fe XIV	1–514	$3s^2\,3p^3({}^4_3S)\ {}^4S^o_{3/2} - 3s^2\,3p^2({}^3_2P)\ {}^3P4d\ {}^4D_{3/2}$	0.27	–	64.48	65.386		?
Fe XIV	4–612	$3s^2\,3p^3({}^2_1P)\ {}^2P^o_{1/2} - 3s^2\,3p^2({}^1_0S)\ {}^1S4d\ {}^2D_{3/2}$	0.25	–	64.19	65.378		?
Fe XIV	1–492	$3s^2\,3p^3({}^4_3S)\ {}^4S^o_{3/2} - 3s^2\,3p^2({}^3_2P)\ {}^3P4d\ {}^2P_{3/2}$	0.25	–	65.16	66.103		?
Fe XIV	3–517	$3s^2\,3p^3({}^2_3D)\ {}^2D^o_{5/2} - 3s^2\,3p^2({}^3_2P)\ {}^3P4d\ {}^4D_{5/2}$	0.22	–	66.53	67.382		?
Fe XIV	1–501	$3s^2\,3p^3({}^4_3S)\ {}^4S^o_{3/2} - 3s^2\,3p^2({}^3_2P)\ {}^3P4d\ {}^4P_{1/2}$	0.21	–	64.80	65.712		?
Fe XIV	1–486	$3s^2\,3p^3({}^4_3S)\ {}^4S^o_{3/2} - 3s^2\,3p^2({}^3_2P)\ {}^3P4d\ {}^4F_{3/2}$	0.2	–	65.39	66.380		?
Fe XIV	1–495	$3s^2\,3p^3({}^4_3S)\ {}^4S^o_{3/2} - 3s^2\,3p^2({}^3_2P)\ {}^3P4d\ {}^2P_{1/2}$	0.2	–	64.98	65.910		?
Fe XIV	5–581	$3s^2\,3p^3({}^2_1P)\ {}^2P^o_{3/2} - 3s^2\,3p^2({}^1_2D)\ {}^1D4d\ {}^2S_{1/2}$	0.15	67.164 No	65.94	66.950		?
Fe XIV	2–552	$3s^2\,3p^3({}^2_3D)\ {}^2D^o_{3/2} - 3s^2\,3p^2({}^1_2D)\ {}^1D4d\ {}^2D_{5/2}$	4.9×10^{-2}	66.221 No	65.17	66.072		?

3.1.2. Transition probabilities with uncertainty estimates

By comparing two sets of theoretical transition data obtained with two different methods (MCDHF and RMBPT), or by comparing the two sets of line strengths obtained using the length l and velocity gauges v from the MCDHF method, we used the uncertainty estimation method suggested by Kramida[94,95] to classify theoretical transition rates of the ions in different isoelectronic sequences listed in Tables 1 and 3, according to the NIST ASD[65] terminology (AA $\leq 1\%$, A+ $\leq 2\%$, A $\leq 3\%$, B+ $\leq 7\%$, B $\leq 10\%$, C+ $\leq 18\%$, C $\leq 25\%$, D+ $\leq 40\%$, D $\leq 50\%$, and E $> 50\%$).

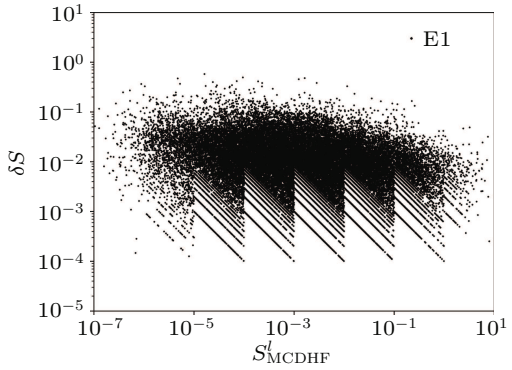


Fig. 2. The relative difference $\delta S = \left|S^{l}_{\mathrm{MCDHF}} - S^{v}_{\mathrm{MCDHF}}\right| / \max(S^{l}_{\mathrm{MCDHF}}, S^{v}_{\mathrm{MCDHF}})$ of line strengths S^{l}_{MCDHF} and S^{v}_{MCDHF} for E1 transitions with BF $\geq 10^{-5}$ among the lowest 702 levels of the $n \leq 5$ configurations.

Here, in Fig. 2 we show this uncertainty estimation method by comparing the two sets of E1 line strengths obtained using the length (l) and velocity (v) gauges from the MCDHF method in Fe XIII. Defining the difference δS between the two forms as $\delta S = \left|S^{l}_{\mathrm{MCDHF}} - S^{l}_{\mathrm{MCDHF}}\right| / \max(S^{l}_{\mathrm{MCDHF}}, S^{l}_{\mathrm{MCDHF}})$, the averaged uncertainties δS_{av} for line strengths S of E1 transitions in Fe XIII in various ranges of S are assessed to 1% for $S \geq 10^{-1}$; 1.3% for $10^{-1} > S \geq 10^{-2}$; 2.6% for $10^{-2} > S \geq 10^{-3}$; 5% for $10^{-3} > S \geq 10^{-4}$; 7% for $10^{-4} > S \geq 10^{-5}$, and 11% for $10^{-5} > S \geq 10^{-6}$. Then, the larger of δS_{av} and $\left|\delta S_{ji}\right|$ is accepted as the uncertainty of each particular line strength. About 7% of E1 S values in Fe XIII have uncertainties of $\leq 1\%$ (AA), 18% have uncertainties of $\leq 2\%$ (A+), 24% have uncertainties of $\leq 3\%$ (A), 44% have uncertainties of $\leq 7\%$ (B+), 1% have uncertainties of $\leq 10\%$ (B), 5% have uncertainties of $\leq 18\%$ (C+), 0.5% have uncertainties of $\leq 25\%$ (C), and 0.1% have uncertainties of $\leq 40\%$ (D+), while only 0.1% have uncertainties of $> 40\%$ (D and E).

3.2. Highly charged tungsten ions

3.2.1. M-shell and N-shell tungsten ions

For the highly charged tungsten ions, our research group has already devoted to the study of the excitation energies, E1, M1, E2, M2, and E3 transition properties for M-shell (open 3p- and 3d-subshell) and N-shell (open 4p-subshell) tungsten ions[29,30,34,96–101] by using the RMBPT and MCDHF methods. The targeted configurations and the number of studied states for each tungsten ion are summarized in Table 5. We briefly review our previous works below.

Table 5. Ions, targeted configurations, methods of the calculations, and the number (N) of studied states for each ion. In the table $l = 0, \ldots, n-1$. The excitation energies, E1, M1, E2, M2, and E3 transition properties are studied for the targeted states in our previous works listed in the last column.

Ions	Configurations	Methods	N	Refs.
Al-like W	$3l^3$	RMBPT&MCDHF	148	this work, [30]
Si-like W	$3l^4$	RMBPT&MCDHF	15	[30]
P-like W	$3l^5$	RMBPT&MCDHF	16	[30]
S-like W	$3s^23p^4$, $3s^23p^33d$, $3s^23p^23d^2$, $3s3p^23d^3$, $3s^23p3d^3$, $3s3p^43d$, $3s3p^33d^2$, $3p^43d^2$, $3p^53d$, $3p^6$	RMBPT&MCDHF	88	[29,30]
Cl-like W	$3s^23p^5$, $3s^23p^43d$, $3s^23p^33d^2$, $3s^23p^23d^3$, $3s3p^53d$, $3s3p^43d^2$, $3s3p^33d^3$, $3p^43d^3$, $3s3p^6$, $3s3p^23d^4$	RMBPT&MCDHF	41	[30]
Ar-like W	$3s^23p^6$, $3s^23p^53d$, $3s^23p^43d^2$, $3s3p^43d^3$, $3s^23p^33d^3$, $3s3p^63d$, $3s3p^53d^2$, $3s^23p^23d^4$	RMBPT&MCDHF	40	[30]
K-like W	$3s^23p^63d$, $3s3p^63d^2$, $3s^23p^43d^3$ $3s^23p^53d^2$, $3s^23p^33d^4$, $3s3p^53d^3$	RMBPT&MCDHF	176	[96]
Ca-like W	$3s^23p^63d^2$, $3s3p^63d^3$, $3s^23p^43d^4$, $3s^23p^53d^3$, $3s^23p^33d^5$	RMBPT&MCDHF	158	[96]
Sc-like W	$3s^23p^63d^3$, $3s3p^63d^4$, $3s^23p^43d^5$, $3s^23p^53d^4$, $3s^23p^33d^6$	RMBPT&MCDHF	171	[96]
Ti-like W	$3s^23p^63d^4$, $3s3p^63d^5$, $3s^23p^43d^6$, $3s^23p^53d^5$, $3s^23p^33d^7$	RMBPT&MCDHF	190	[96]
V-like W	$3s^23p^63d^5$, $3s3p^63d^6$, $3s^23p^43d^7$, $3s^23p^53d^6$	RMBPT&MCDHF	162	[96]
Cr-like W	$3s^23p^63d^6$, $3s3p^63d^7$, $3s^23p^43d^8$, $3s^23p^53d^7$, $3s^23p^33d^9$, $3s3p^53d^8$	RMBPT&MCDHF	190	[96]

Table 5. (*Continued*).

Ions	Configurations	Methods	N	Refs.
Mn-like W	$3s^23p^63d^7$, $3s3p^63d^8$, $3s^23p^43d^9$, $3s3p^43d^{10}$, $3p^63d^9$, $3s^23p^53d^8$, $3s^23p^33d^{10}$, $3s3p^53d^9$, $3p^53d^{10}$	RMBPT&MCDHF	79	[96]
Fe-like W	$3s^23p^63d^8$, $3s3p^63d^9$, $3s^23p^43d^{10}$, $3p^63d^{10}$, $3s^23p^53d^9$, $3s3p^53d^{10}$	RMBPT&MCDHF	25	[96]
Co-like W	$3s^23p^63d^9$, $3s3p^63d^{10}$, $3s^23p^63d^84s$, $3s^23p^63d^84d$, $3s^23p^53d^94p$, $3s^23p^53d^94f$, $3s^23p^43d^{10}4p$, $3s3p^63d^94s$, $3s^23p^53d^{10}$, $3s^23p^63d^84p$, $3s^23p^63d^84f$, $3s^23p^53d^94s$, $3s^23p^53d^94d$	RMBPT&MCDHF	5	[34,97]
Ga-like W	$4s^24p$, $4s^24d$, $4s4p^2$, $4s^24f$, $4s4p4d$, $4p^3$	RMBPT&MCDHF	42	[98]
Ge-like W	$4s^24p^2$, $4s^24p4d$, $4s4p^3$	RMBPT&MCDHF	27	[98]
As-like W	$4s^24p^3$, $4s^24p^24d$, $4s4p^4$	RMBPT&MCDHF	86	[98,99]
Se-like W	$4s^24p^4$, $4s^24p^34d$, $4s4p^5$	RMBPT&MCDHF	47	[98,100]
Kr-like W	$4s^24p^6$, $4s^24p^54d$	RMBPT&MCDHF	13	[101]

In our works for M-shell and N-shell tungsten ions,[29,30,34,96–101] atomic properties (of $n = 3$ states for M-shell and $n = 4$ states for N-shell) including excitation energies, wavelengths, and transition properties from Al-like W^{61+} through Co-like W^{47+}, Ga-like W^{43+} through Se-like W^{40+}, and W^{38+} ions are calculated and cross-checked by using the RMBPT and MCDHF approaches. The two datasets are in excellent agreement with each other on the order of 0.01% for M-shell and 0.1% for N-shell tungsten ions. Our theoretical results are in good agreement with experiments and show a clear improvement of accuracy over previous calculations.[5,6,102–113] And our calculations achieve spectroscopic accuracy to assist spectroscopists in their assignment and direct identification. Based on our RMBPT and MCDHF calculations and CRM simulations, we also give suggestions of assignments for all of the unidentified 28 spectral lines (a significant fraction, around sixty percent) of the $n = 3 \rightarrow 3$ transitions measured by Lennartsson *et al.*[114]

Additionally, the contributions of electron correlation, the Breit interaction, the higher-order frequency-dependent retardation correction, and the leading QED corrections to excitation energies (transition wavelengths, and radiative rates) are also studied in detail. In the study for Al-like W^{61+} through Co-like W^{47+} ions, we point out that the Breit interaction and QED corrections (the corrections beyond the Dirac–Coulomb Hamiltonian), respectively, play an important role on the 3p–3d and 3s–3p excitation energies. The CV correlation involving the 2p and 2s core electrons and the higher-order retardation corrections beyond the Breit interaction should also not be ignored for getting results with spectroscopic accuracy. In the study for Ga-like W^{43+} through Kr-like W^{38+} ions, we also find that the CV correlation of 3d and 3p is important for reaching close to spectroscopic accuracy for the transition energies.

Especially, we investigate in detail the three different methods to estimate the SE corrections. The first one is that SE corrections are obtained based on a screened hydrogenic approximation in the current GRASP2K package[22] (usually called GRASP2K). The second one is a screening approximation based on the Welton interpretation[115] and implemented in GRASP2K by Lowe *et al.*,[116] starting from the latest available hydrogenic values[117,118] modified to account for finite-nuclear-size effects[119,120] (usually called Welton). The last one is a model QED operator, which also includes the non-local QED part to evaluate the SE corrections for many-electron atomic systems, has been developed by Shabaev *et al.*[31,32] (usually called ModelQED). Based on our systematic assessment,[29,30,34] the Welton and ModelQED methods are more recommended to estimate the SE potential for highly-charged tungsten ions than the GRASP2K method.

3.2.2. Excitation energies for Al-like W^{61+}

In the present MCDHF calculations, the QED corrections are estimated using the three different models, i.e., GRASP2K, Welton, and ModelQED (see Refs. [29,30] for details). And the corresponding MCDHF results (labelled GRASP2K, Welton, and ModelQED, respectively) are compared with the experimental values[121,122] in Table 6. The corresponding differences $\Delta E_{\text{Theo.}} = E_{\text{Theo.}} - E_{\text{Expt.}}$ (in cm^{-1}) are listed as well. From Table 6, it is found that the Welton and ModelQED excitation energies are in general within or close to the experimental estimated uncertainties, with average differences $\pm$ standard deviations of -672 ± 1441 cm^{-1} ($-0.018\% \pm 0.043\%$) and -331 ± 1594 cm^{-1} ($-0.006\% \pm 0.052\%$), respectively, for the 7 levels listed in Table 6. However, the GRASP2K excitation energies differ from the experimental values by -1468 ± 1208 cm^{-1} ($-0.052\% \pm 0.050\%$). As observed in our recent works,[29,30] the values from the Welton and ModelQED calculations are generally closer to the experimental values than the values from the GRASP2K calculation. In the following, the MCDHF results will be all based on the ModelQED model which turns out to be the best model for describing the self-energy QED correction.

Table 6. Excitation energies (E, in cm^{-1}) from the present MCDHF calculations compared with the experimental values (expt).[121,122] The estimated uncertainty of the experimental value for each level is reported in brackets in the Expt column. In the present MCDHF calculations, the QED corrections are estimated by using the three different models, i.e., GRASP2K, Welton, and ModelQED (see Refs. [29,30] for details). The corresponding differences $\Delta E_{\text{Theo.}} = E_{\text{Theo.}} - E_{\text{Expt.}}$ (in cm^{-1}) are also listed.

Key	Level	E_{expt}	E_{GRASP2K}	E_{Welton}	E_{ModelQED}	$\Delta E_{\text{GRASP2K}}$	ΔE_{Welton}	$\Delta E_{\text{ModelQED}}$
1	$3s^23p\ ^2P_{1/2}$	0	0	0	0	0	0	0
2	$3s3p^2\ ^4P_{1/2}$	1350600(400)	1348840	1350721	1351275	–1760	121	675
3	$3s^23p\ ^2P_{3/2}$	2933400(800)	2931330	2930838	2930806	–2070	–2562	–2594
4	$3s3p^2\ ^4P_{3/2}$	4035500(1600)	4035765	4037123	4037609	265	1623	2109
6	$3s3p^2\ ^2D_{3/2}$	4355200(1100)	4352798	4353795	4354193	–2402	–1405	–1007
7	$3s3p^2\ ^2P_{1/2}$	4436000(800)	4433361	4434732	4435298	–2639	–1268	–702
8	$3s^23d\ ^2D_{3/2}$	4817900(900)	4817699	4817362	4817434	–201	–538	–466

In our previous work for tungsten ions with an open 3p-subshell,[30] only excitation energies and wavelengths for a few levels are provided. As a complement, the complete results incorporating excitation energies, E1, M1, E2, and M2 transition properties, and level lifetimes for the lowest 148 levels belonging to the $3l^3$ configurations for Al-like W^{61+} from the RMBPT and MCDHF calculations are presented in this work. The details of the calculations have already been explained in Ref. [30] and do not repeat here.

We also ought to resume the previous relevant theoretical studies. Using the older GRASP package (GRASP89)[124] and the FAC,[26] Aggarwal and Keenan[103] calculated excitation energies, radiative rates, and lifetimes for W^{61+}. Also using the GRASP89 code,[123] Xu *et al.*[104] studied excitation energies, wavelengths and transition probabilities for W^{61+}. The excitation energies and wavelengths for only a few $n = 3$ levels of W^{61+} were provided by Chen and Cheng[106] using the RCI method. Ekman *et al.*[124] also calculated excitation energies and transition probabilities for W^{61+} using the RMBPT and MCDHF methods.

For comparison, the present RMBPT and MCDHF excitation energies for Al-like W^{61+} as well as the compiled data from the NIST ASD[125] are listed in Table 7. The two theoretical data sets (GRASP89 and FAC) reported by Aggarwal and Keenan,[104] the theoretical results provided by Xu *et al.* (MCDHF2),[106] and the values (RCI) calculated by Chen and Cheng[107] are also included in Table 7.

Table 7. Comparison of the excitation energies (E, in cm^{-1}) from the present RMBPT and MCDHF, from the previous works (GRASP89 and FAC: from Aggarwal and Keenan;[103] MCDHF2: from Xu *et al.*;[104] RCI: from Chen and Cheng[106]), and from the measurements.[121,122] The NIST compiled values reported in square brackets are determined by semi-empirical parametric calculations using Cowan's code. The rest of the NIST values are deduced from measured lines. The number reported in parenthesis, after the experimental wavelength, is the estimated experimental uncertainty. The present RMBPT and MCDHF level lifetimes (τ, in s^{-1}) are also listed. The excitation energies and lifetimes from the present RMBPT and MCDHF calculations shown in this table are published in their entirety online.

Key	Level	E_{NIST}	E_{RMBPT}	E_{MCDHF}	E_{GRASP89}	E_{FAC}	E_{MCDHF2}	E_{RCI}	τ_{RMBPT}	τ_{MCDHF}
1	$3s^23p\ ^2P_{1/2}$	0	0	0	0	0	0	0		
2	$3s3p^2\ ^4P_{1/2}$	1350600(400)	1350929	1351275	1364802	1351442	1348131	1350575	2.66×10^{-11}	2.65×10^{-11}
3	$3s^23p\ ^2P_{3/2}$	2933400(800)	2931756	2930806	2929418	2932205	2929446	2932148	2.02×10^{-9}	2.02×10^{-9}
4	$3s3p^2\ ^4P_{3/2}$	4035500(1600)	4038504	4037609	4045803	4036194	4033877	4037611	7.20×10^{-11}	7.21×10^{-11}
5	$3s3p^2\ ^2D_{5/2}$	[4182000](5000)	4184693	4184039	4194325	4184255	4183114		7.19×10^{-11}	7.18×10^{-11}
6	$3s3p^2\ ^2D_{3/2}$	4355200(1100)	4354716	4354193	4364149	4355110	4349474	4352571	1.27×10^{-12}	1.27×10^{-12}
7	$3s3p^2\ ^2P_{1/2}$	4436000(800)	4435669	4435298	4451343	4440516	4433339	4436049	3.60×10^{-13}	3.60×10^{-13}
8	$3s^23d\ ^2D_{3/2}$	4817900(900)	4817430	4817434	4827551	4820367	4820751	4811662	2.76×10^{-13}	2.75×10^{-13}
9	$3s^23d\ ^2D_{5/2}$	[5406000](5000)	5408822	5408402	5410144	5405142			3.53×10^{-12}	3.52×10^{-12}
10	$3p^3\ ^2P_{3/2}$		5678200	5677888	5694815	5676486			2.76×10^{-12}	2.76×10^{-12}
11	$3s3p3d\ ^4F_{3/2}$		5785858	5785576	5805724	5783128			2.67×10^{-12}	2.66×10^{-12}
12	$3s3p3d\ ^4F_{5/2}$		5884110	5883974	5897887	5879338			3.66×10^{-11}	3.65×10^{-11}
13	$3s3p3d\ ^4D_{1/2}$		6097112	6097266	6115559	6097185			4.30×10^{-13}	4.29×10^{-13}
14	$3s3p3d\ ^4D_{3/2}$		6150991	6151183	6171589	6152404			3.00×10^{-13}	2.99×10^{-13}
15	$3s3p3d\ ^4P_{5/2}$		6547177	6546688	6557736	6540361			3.61×10^{-12}	3.60×10^{-12}
16	$3s3p3d\ ^4F_{7/2}$		6661171	6660947	6673822	6656041			4.77×10^{-12}	4.76×10^{-12}
17	$3s3p3d\ ^2F_{5/2}$		6743848	6743855	6758219	6740065			3.96×10^{-12}	3.95×10^{-12}
18	$3s3p3d\ ^2D_{3/2}$		6783035	6783080	6800110	6781188			1.54×10^{-12}	1.53×10^{-12}
19	$3s3p^2\ ^4P_{5/2}$	[7064000](5000)	7067483	7065832	7074876	7067647			1.44×10^{-12}	1.44×10^{-12}
20	$3s3p^2\ ^2S_{1/2}$	[7365000](5000)	7368166	7366908	7380575	7372293			5.03×10^{-13}	5.02×10^{-13}
21	$3p^2(3P)3d\ ^4F_{3/2}$		7390343	7390560	7437099	7390063			1.46×10^{-12}	1.37×10^{-12}
22	$3s3p^2\ ^2P_{3/2}$	[7405000](5000)	7428967	7428015	7428367	7434707			2.85×10^{-13}	2.88×10^{-13}

The NIST compiled values in square brackets are determined from semi-empirical calculations by Kramida[126] using Cowan's code.[127] The other NIST values are deduced from measured lines that were observed using the EBIT facilities.[121,122] For each level, the number reported in parenthesis, after the NIST excitation level energy, is the estimated accuracy provided by the NIST ASD. It can be seen from Table 7 that the uncertainty of the NIST values quoted in square brackets is 5000 cm^{-1}, whereas the NIST values deduced by measured lines are much more accurate (400 cm^{-1}–1600 cm^{-1}).

The energy differences, $\Delta E = E_{\rm Others} - E_{\rm RMBPT}$, of the different theoretical excitation energies and the NIST compiled values from the present RMBPT results are shown in Fig. 3. The present MCDHF and RMBPT are in good agreement with each other, with an average difference with the standard deviation of $-370\ cm^{-1} \pm 518\ cm^{-1}$ ($-0.007\% \pm 0.01\%$) for the lowest 22 levels listed in Table 7. The present RMBPT and MCDHF results agree with the NIST compiled experimental values within 3000 cm^{-1} (0.07%) and 2600 cm^{-1} (0.09%), respectively, which are generally within or closed to the NIST estimated uncertainties. However, the GRASP89 results of Aggarwal and Keenan[103] deviate from the NIST compiled experimental values by up to $\simeq 14000\ cm^{-1}$ (100%) and not less than $\simeq -4000\ cm^{-1}$ (0.1%). On the contrary, their FAC results agree more with the NIST compiled measured values than the GRASP89 results, with the differences by up to 4500 cm^{-1} (0.1%). Similarly, the excitation energies calculated by Xu *et al.*[104] and Chen and Cheng[106] are lower than the NIST compiled measured values by up to $\simeq 5700\ cm^{-1}$ (0.1%) and 6200 cm^{-1} (0.1%), respectively.

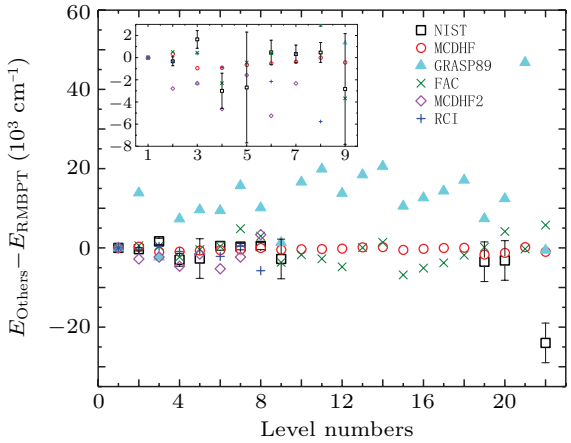


Fig. 3. The deviations for the excitation energies in Al-like W^{61+} between the different theoretical (the present RMBPT and MCDHF, as well as the previous works: GRASP89 and FAC: from Aggarwal and Keenan;[103] MCDHF2: from Xu *et al.*;[104] RCI: from Chen and Cheng[106]), and experimental values.[121,122] Vertical error bars are experimental uncertainties. The inset shows the enlargement of differences for the lowest 9 levels.

The differences between the previous calculations of excitation energies[103,104,106] and the measured values compiled in NIST are several times or more than one order of magnitude larger than the corresponding differences calculated for the present RMBPT and MCDHF results. This indicates that the present theoretical excitation energies of Al-like W^{61+} are highly accurate and represent a great improvement on the latest theoretical results.[103,104,106]

Looking at the NIST values that are reported in square brackets to mark their origin from semi-empirical parametric calculations, their differences with the present theoretical values are up to 24000 cm^{-1}. For this reason, our RMBPT and MCDHF excitation energies, compared with these NIST compiled values, also represent a substantial improvement in accuracy. As already mentioned in our recent work for S-like W^{58+},[29] we, therefore, recommend the use of our theoretical values (not only for W^{61+} and W^{58+}, but also for other highly-charged tungsten ions) for updating these NIST semi-empirical data, and even suggest their use as input data for a new parametric fit using Cowan's code, which would increase dramatically the accuracy and quality of the NIST compiled values.

The excitation energies of the lowest 148 levels from the present RMBPT and MCDHF are published in their entirety online. Our two datasets can cross-check with each other, and the average difference with the standard deviation between them for the lowest 148 levels is found to be $-661\ cm^{-1}$ $\pm 513\ cm^{-1}$ ($-0.006\% \pm 0.006\%$).

3.2.3. Transition properties for Al-like W^{61+}

In Table 8, wavelengths (λ, in Å), transition rates (A, in s^{-1}), line strengths (S, in a.u.), and weighted oscillator strength (gf, dimensionless) obtained from the present RMBPT and MCDHF calculations for the E1, E2, M1, and M2 transitions among the lowest 148 levels, with radiative branching ratios (BRs) over 0.1% for Al-like W^{61+}, are presented. The last column represents the estimated accuracy of the S-values using the terminologies of the NIST ASD.[125] Our transition properties are given in the Babushkin gauge.

There are in total 3270 transitions originating from Al-like W^{61+} with BRs over 0.1% in Table 8. These transitions lie in a wide wavelength range from 7 Å to 230 Å, and all of them are in x-ray and EUV ranges. The average difference with the standard deviation between our two data sets for these 3270 transitions is found to be $-0.0003\% \pm 0.03\%$ for wavelengths, $-2\% \pm 13\%$ for transition rates, $-2\% \pm 13\%$ for weighted oscillator strength, and $-0.0002\% \pm 0.001\%$ for line strengths.

Table 8. The present RMBPT and MCDHF wavelengths (λ, in Å), transition rates (A, in s^{-1}), line strength (S, in a.u.), and weighted oscillator strength (gf, dimensionless), with radiative branching ratios (BRs) over 0.1% for Al-like W^{61+}. The last column represents the estimated accuracies of the S-values using the terminologies of the NIST ASD.[125] This table is available in its entirety online. Some selected transitions are shown here for guidance regarding their form and content.

LL	UL	TM	λ_{RMBPT}	λ_{MCDHF}	A_{RMBPT}	A_{MCDHF}	S_{RMBPT}	S_{MCDHF}	gf_{RMBPT}	gf_{MCDHF}	BRs	Acc. (S)
1	2	E1	74.023	74.004	3.840×10^{10}	3.774×10^{10}	1.537×10^{-2}	1.510×10^{-2}	6.308×10^{-2}	6.198×10^{-2}	1.00×10^{0}	B+
2	3	E1	63.259	63.310	2.735×10^{8}	2.702×10^{8}	1.367×10^{-4}	1.354×10^{-4}	6.562×10^{-4}	6.496×10^{-4}	5.49×10^{-1}	B+
1	4	E1	24.762	24.767	1.186×10^{10}	1.162×10^{10}	3.554×10^{-4}	3.484×10^{-4}	4.360×10^{-3}	4.273×10^{-3}	8.37×10^{-1}	B+
3	4	E1	90.356	90.350	2.083×10^{9}	2.042×10^{9}	3.034×10^{-3}	2.974×10^{-3}	1.020×10^{-2}	9.998×10^{-3}	1.47×10^{-1}	B+
3	5	E1	79.812	79.794	1.419×10^{10}	1.392×10^{10}	2.136×10^{-2}	2.094×10^{-2}	8.128×10^{-2}	7.973×10^{-2}	1.00×10^{0}	B+
1	6	E1	22.964	22.966	7.821×10^{11}	7.658×10^{11}	1.870×10^{-2}	1.831×10^{-2}	2.474×10^{-1}	2.422×10^{-1}	9.69×10^{-1}	B+
3	6	E1	70.276	70.255	2.539×10^{10}	2.487×10^{10}	1.740×10^{-2}	1.703×10^{-2}	7.520×10^{-2}	7.362×10^{-2}	3.14×10^{-2}	B+
1	7	E1	22.545	22.546	2.808×10^{12}	2.749×10^{12}	3.176×10^{-2}	3.111×10^{-2}	4.280×10^{-1}	4.191×10^{-1}	9.89×10^{-1}	B+
3	7	E1	66.493	66.468	3.246×10^{10}	3.183×10^{10}	9.420×10^{-3}	9.226×10^{-3}	4.304×10^{-2}	4.216×10^{-2}	1.14×10^{-2}	B+
1	8	E1	20.758	20.758	3.717×10^{12}	3.633×10^{12}	6.563×10^{-2}	6.415×10^{-2}	9.604×10^{-1}	9.387×10^{-1}	1.00×10^{0}	B+
3	8	E1	53.031	53.005	2.925×10^{8}	2.770×10^{8}	8.611×10^{-5}	8.143×10^{-5}	4.932×10^{-4}	4.666×10^{-4}	7.87×10^{-5}	B
3	9	E1	40.370	40.362	2.915×10^{11}	2.840×10^{11}	5.680×10^{-2}	5.531×10^{-2}	4.272×10^{-1}	4.162×10^{-1}	1.00×10^{0}	B+
2	10	E1	23.109	23.113	2.983×10^{11}	2.908×10^{11}	7.267×10^{-3}	7.088×10^{-3}	9.552×10^{-2}	9.315×10^{-2}	8.03×10^{-1}	B+
4	10	E1	60.986	60.965	2.133×10^{10}	2.087×10^{10}	9.551×10^{-3}	9.335×10^{-3}	4.756×10^{-2}	4.651×10^{-2}	5.74×10^{-2}	B+
5	10	E1	66.956	66.941	3.955×10^{10}	3.857×10^{10}	2.344×10^{-2}	2.284×10^{-2}	1.063×10^{-1}	1.036×10^{-1}	1.07×10^{-1}	B+
6	10	E1	75.558	75.546	5.049×10^{9}	4.927×10^{9}	4.299×10^{-3}	4.194×10^{-3}	1.728×10^{-2}	1.686×10^{-2}	1.36×10^{-2}	B+
7	10	E1	80.481	80.477	6.837×10^{9}	6.685×10^{9}	7.036×10^{-3}	6.879×10^{-3}	2.656×10^{-2}	2.596×10^{-2}	1.84×10^{-2}	B+
8	10	E1	116.178	116.218	4.010×10^{8}	3.906×10^{8}	1.242×10^{-3}	1.211×10^{-3}	3.246×10^{-3}	3.164×10^{-3}	1.08×10^{-3}	B+

Figures 4 and 5 respectively show the differences between the present RMBPT and MCDHF wavelengths and transition rates for all of the transitions listed in Table 8. As we can see, 84% of our two datasets for transition wavelengths agree with each other within 0.03%, and 84% of our two datasets for transition rates agree with each other within 10%.

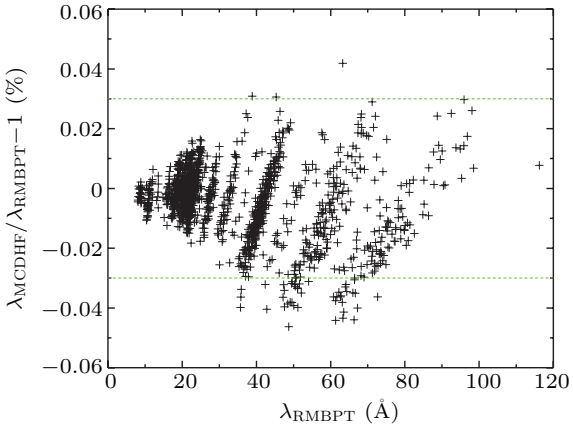


Fig. 4. The deviations between the present RMBPT and MCDHF transition wavelengths for Al-like W^{61+}.

Furthermore, the uncertainty estimation method, proposed by Kramida,[94,95] is used to classify the accuracy of the present RMBPT and MCDHF S-values, according to the NIST ASD[125] terminology (AA $\leq$ 1%, A+ $\leq$ 2%, A $\leq$ 3%, B+ $\leq$ 7%, B $\leq$ 10%, C+ $\leq$ 18%, C $\leq$ 25%, D+ $\leq$ 40%, D $\leq$ 50%, and $E >$ 50%). The estimation details can be seen in our recent works.[63,96] For the 2673 E1 transitions originating from W^{61+} listed in Table 8, about 55.2% have uncertainties 3% $\leq \delta \leq$ 7% (B+), 15.8% with $\delta \leq$ 10% (B), 13.2% with $\delta \leq$ 18% (C+), 9.6% with $\delta \leq$ 25% (C), and only 6.2% with $\delta \geq$ 25% (D, D+, and E). It should be noted that the uncertainty of the S-value of each transition is estimated by including all transitions of each ion considered, without any restriction on the line intensity values in the uncertainty estimation procedure, although only transitions with BRs over 0.1% are provided in Table 8. The uncertainties of the present RMBPT and MCDHF S-values of E2, M1, and M2 transitions are also estimated as for the E1 ones.

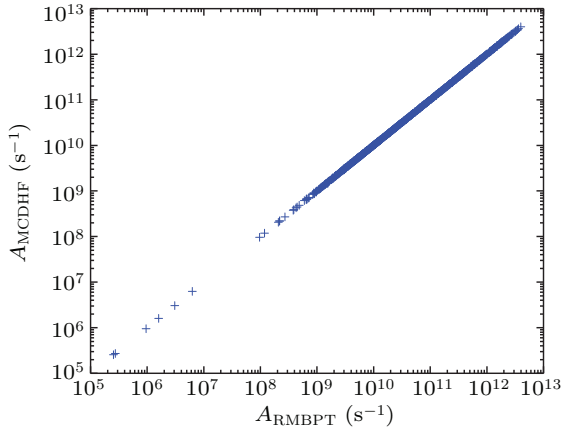


Fig. 5. The comparison of the present RMBPT and MCDHF transition rates for Al-like W^{61+}.

3.2.4. Level lifetimes for Al-like W^{61+}

In Table 7, the present RMBPT and MCDHF level lifetimes for the lowest 22 levels in Al-like W^{61+} are listed, and the complete datasets for the lowest 148 levels are also published in their entirety online. Figure 6 shows the differences between the present RMBPT and MCDHF level lifetimes for the lowest 148 levels in Al-like W^{61+}. One can see that our two data sets are in good agreement with each other, and most

of the differences between them are within 0.3%, even though the present MCDHF level lifetimes are generally lower than RMBPT ones.

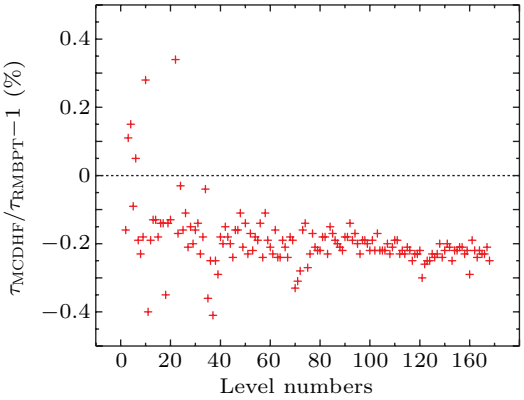


Fig. 6. The comparison of the present RMBPT and MCDHF level lifetimes for Al-like W^{61+}.

4. Conclusions and outlook

Employing two different and independent methods, i.e., MCDHF and RMBPT, we have systematically studied the atomic radiative data such as excitation energies, transition wavelengths, radiative rates, and level lifetimes for the ions with $Z \leq 42$ and tungsten ($Z = 74$) ions to meet demands of astrophysical and fusion plasmas. In this work, we mainly review our previous works performed in the past decade. As a complement/extension to our previous works for highly charged tungsten ions with open M-shell and open N-shell, we also present and discuss our complete RMBPT and MCDHF calculations for the excitation energies, wavelengths, E1, M1, E2, and M2 transition properties, and level lifetimes for the lowest 148 levels belonging to the $3l^3$ configurations in Al-like W^{61+}. And the calculations for L-shell, N-shell, and lower-charged tungsten ions will be reported in future works.

By cross-checking two datasets from our RMBPT and MCDHF calculations and comparing them with other theoretical calculations and available experiments in the literature, we summarize the uncertainties of our systematical calculations here. For K- and L- shells ions with $Z \leq 42$ the uncertainty of calculated transition wavelengths is about 0.01%–0.05%. For the M-shell ions with $Z \leq 42$, the uncertainty of calculated transition wavelengths is on the order of 0.1%. For the M-shell tungsten ions, the uncertainty of calculated $n = 3 \rightarrow 3$ transition wavelengths is about 0.01%–0.05%. And for the N-shell tungsten ions, the uncertainty of calculated $n = 4 \rightarrow 4$ transition wavelengths is on the order of 0.1%.

We expect that our theoretical calculations with high precision provide precise benchmarks for other theoretical calculations and experimental measurements as well as applications for abundance analysis, simulation, and diagnostics in astrophysical and fusion plasmas.

Additionally, in our recent works[128,129] we mainly focused on discussing in detail how to improve the efficiency of the RSCF procedure of the MCDHF method and the RCI calculations. For the RSCF, the routines for calculating the direct and exchange potentials and the Lagrange multipliers are redesigned.[128] For the RCI, regrouping CSFs and introducing CSF generators allow for a substantial reduction of the computational load.[129] Compared with the original GRASP codes, our contributions reduce CPU times by a few tens or more factors. A large amount of atomic data of high accuracy for more complex ions is expected to be provided in the future.

Data availability statement

The data that support the findings of this study are openly available in Science Data Bank at https://doi.org/10.57760/sciencedb.10569.

Acknowledgements

We acknowledge the support from the National Natural Science Foundation of China (Grant Nos. 12074081 and 12104095). Many works reviewed here are accomplished in close collaboration with other groups, such as members of the CompAS group, and M. F. Gu (author of the FAC code), etc.

References

[1] Del Zanna G and Mason H E 2018 *Living Rev. Sol. Phys.* **15** 5
[2] Hawryluk R, Campbell D, Janeschitz G, *et al.* 2009 *Nucl. Fusion* **49** 065012
[3] Yao D, Luo G, Du S, Cao L, Zhou Z, Xu T, Ji X, Liu C, Liang C, Li Q,Wang W, Zhao S, Xu Y, Li L,Wang Z, Qi X X M, Wang S and Li J 2015 *Fusion Eng. Des.* **98–99** 1692
[4] Zhang L, Morita S, Wu Z, Xu Z, Yang X, Cheng Y, Zang Q, Liu H, Liu Y, Zhang H, Ohishi T, Chen Y, Xu L, Wu C, Duan Y, Gao W, Huang J, Gong X and Hu L 2019 *Nucl. Instrum. Methods Phys. Res. Sect. A* **916** 169
[5] Froese Fischer C, Gaigalas G and Jönsson P 2017 *Atoms* **5** 7
[6] Safronova M S, Safronova U I, Porsev S G, Kozlov M G and Ralchenko Y 2018 *Phys. Rev. A* **97** 012502
[7] Beiersdorfer P, Clementson J, Dunn J, Gu M F, Morris K, Podpaly Y, Wang E, Bitter M, Feder R, Hill K W, Johnson D and Barnsley R 2010 *J. Phys. B: At., Mol. Opt. Phys.* **43** 144008
[8] Beiersdorfer P, Clementson J and Safronova U I 2015 *Atoms* **3** 260
[9] Rzadkiewicz J, Yang Y, Kozioł K, O'Mullane M G, Patel A, Xiao J, Yao K, Shen Y, Lu D, Hutton R, Zou Y and Contributors J 2018 *Phys. Rev. A* **97** 052501
[10] Gormezano C, Sips A, Luce T, *et al.* 2007 *Nucl. Fusion* **47** S285
[11] Donné A, Costley A, Barnsley R, *et al.* 2007 *Nucl. Fusion* **47** S337
[12] Clementson J, Beiersdorfer P and Gu M F 2010 *Phys. Rev. A* **81** 012505
[13] Wyart J F and Group T 1985 *Phys. Scr.* **31** 539
[14] Denne B, Hinnov E, Ramette J and Saoutic B 1989 *Phys. Rev. A* **40** 1488
[15] Martinson I and Jupén C 2003 *Phys. Scr.* **68** C123
[16] Myrnäs R, Jupén C, Miecznik G, Martinson I and Denne-Hinnov B 1994 *Phys. Scr.* **49** 429
[17] Hinnov E, TFTR Operating Team, Denne B and JET Operating Team 1989 *Phys. Rev. A* **40** 4357
[18] Barnsley R, O'Mullane M, Ingesson L C and Malaquias A 2004 *Rev. Sci. Instrum.* **75** 3743
[19] Donné A J H, Costley A E, Barnsley R, *et al.* 2007 *Nucl. Fusion.* **47** S337

[20] Grant I P 2007 *Relativistic Quantum Theory of Atoms and Molecules* (New York, NY: Springer Sci. +Bus. Media, LLC)
[21] Froese Fischer C, Godefroid M, Brage T, Jönsson P and Gaigalas G 2016 *J. Phys. B: At., Mol. Opt. Phys.* **49** 182004
[22] Jönsson P, Gaigalas G, Bieroń J, Froese Fischer C and Grant I P 2013 *Comput. Phys. Commun.* **184** 2197
[23] Lindgren I 1974 *J. Phys. B: At. Mol. Opt. Phys.* **7** 2441
[24] Safronova M S, Johnson W R and Safronova U I 1996 *Phys. Rev. A* **53** 4036
[25] Vilkas M J, Ishikawa Y and Koc K 1999 *Phys. Rev. A* **60** 2808
[26] Gu M F 2008 *Can. J. Phys.* **86** 675
[27] Gu M F 2005 *At. Data Nucl. Data Tables* **89** 267
[28] Gu M F, Holczer T, Behar E and Kahn S M 2006 *Astrophys. J.* **641** 1227
[29] Zhang C Y, Wang K, Godefroid M, Jönsson P, Si R and Chen C Y 2020 *Phys. Rev. A* **101** 032509
[30] Zhang C Y, Wang K, Si R, Godefroid M, Jönsson P, Xiao J, Gu M F and Chen C Y 2021 *J. Quant. Spectrosc. Radiat. Transfer* **269** 107650
[31] Shabaev V M, Tupitsyn I I and Yerokhin V A 2013 *Phys. Rev. A* **88** 012513
[32] Shabaev V M, Tupitsyn I I and Yerokhin V A 2015 *Comput. Phys. Commun.* **189** 175
[33] Li M C, Si R, Brage T, Hutton R and Zou Y M 2018 *Phys. Rev. A* **98** 020502
[34] Si R, Guo X L, Brage T, Chen C Y, Hutton R and Froese Fischer C 2018 *Phys. Rev. A* **98** 12504
[35] Olsen J, Godefroid M R, Jönsson P, Malmqvist P Å and Froese Fischer C 1995 *Phys. Rev. E* **52** 4499
[36] Grant I P 1974 *J. Phys. B: At., Mol. Opt. Phys.* **7** 1458
[37] Chen C Y, Wang K, Huang M, Wang Y S and Zou Y M 2010 *J. Quant. Spectrosc. Radiat. Transfer* **111** 843
[38] Li S, Yan J, Li C Y, Si R, Guo X L, Huang M, Chen C Y and Zou Y M 2015 *Astron. & Astrophys.* **583** A82
[39] Si R, Guo X L, Wang K, Li S, Yan J, Chen C Y, Brage T and Zou Y M 2016 *Astron. & Astrophys.* **592** A141
[40] Si R, Li S, Wang K, Guo X L, Chen Z B, Yan J, Chen C Y, Brage T and Zou Y M 2017 *Astron. & Astrophys.* **600** A85
[41] Wang K, Chen Z B, Zhang C Y, Si R, Jönsson P, Hartman H, Gu M F, Chen C Y and Yan J 2018 *Astrophys. J. Supp. Ser.* **234** 40
[42] Wang K, Guo X L, Liu H T, Li D F, Long F Y, Han X Y, Duan B, Li J G, Huang M, Wang Y S, Hutton R, Zou Y M, Zeng J L, Chen C Y and Yan J 2015 *Astrophys. J. Supp. Ser.* **218** 16
[43] Chen Z B and Wang K 2019 *J. Quant. Spectrosc. Radiat. Transf.* **234** 90
[44] Chen Z B, Wang K and Guo X L 2018 *J. Quant. Spectrosc. Radiat. Transf.* **220** 28
[45] Chen Z B and Wang K 2018 *J. Quant. Spectrosc. Radiat. Transf.* **221** 31
[46] Wang K, Song C X, Jönsson P, Ekman J, Godefroid M, Zhang C Y, Si R, Zhao X H, Chen C Y and Yan J 2018 *Astrophys. J. Supp. Ser.* **864** 127
[47] Si R, Zhang C Y, Cheng Z Y, Wang K, Jönsson P, Yao K, Gu M F and Chen C Y 2018 *Astrophys. J. Supp. Ser.* **239** 3
[48] Li Y T, Si R, Li J Q, Zhang C Y, Yao K, Wang K, Gu M F and Chen C Y 2020 *At. Data Nucl. Data Tables* **133–134** 101339
[49] Li J Q, Zhang C Y, Zanna G D, Jönsson P, Godefroid M, Gaigalas G, Rynkun P, Radžiūtė L, Wang K, Si R and Chen C Y 2022 *Astrophys. J. Supp. Ser.* **260** 50
[50] Wang K, Li D F, Liu H T, Han X Y, Duan B, Li C Y, Li J G, Guo X L, Chen C Y and Yan J 2014 *Astrophys. J. Supp. Ser.* **215** 26
[51] Wang K, Si R, Dang W, Jönsson P, Guo X L, Li S, Chen Z B, Zhang H, Long F Y, Liu H T, Li D F, Hutton R, Chen C Y and Yan J 2016 *Astrophys. J. Supp. Ser.* **223** 3
[52] Wang K, Zhang C Y, Jönsson P, Si R, Zhao X H, Chen Z B, Guo X L, Chen C Y and Yan J 2018 *J. Quant. Spectrosc. Radiat. Transf.* **208** 134
[53] Wang K, Wang Y, Zhang C Y, Zhao X H, Chen Z B, Si R, Chen C Y and Yan J 2018 *J. Quant. Spectrosc. Radiat. Transfer* **220** 5
[54] Wang K, Li S, Jönsson P, Fu N, Dang W, Guo X L, Chen C Y, Yan J, Chen Z B and Si R 2017 *J. Quant. Spectrosc. Radiat. Transf.* **187** 375
[55] Wang K, Chen Z B, Zhao X H, Chen C Y and Yan J 2019 *J. Quant. Spectrosc. Radiat. Transf.* **237** 106640
[56] Song C X, Zhang C Y, Wang K, Si R, Godefroid M, Jönsson P, Dang W, Zhao X H, Yan J and Chen C Y 2021 *At. Data Nucl. Data Tables* **138** 101377
[57] Wang K, Jönsson P, Ekman J, Gaigalas G, Godefroid M R, Si R, Chen Z B, Li S, Chen C Y and Yan J 2017 *Astrophys. J. Supp. Ser.* **229** 37
[58] Chen Z B, Guo X L and Wang K 2018 *J. Quant. Spectrosc. Radiat. Transf.* **206** 213
[59] Wang K, Jönsson P, Ekman J, Si R, Chen Z B, Li Y, Chen C Y and Yan J 2017 *J. Quant. Spectrosc. Radiat. Transf.* **194** 108
[60] Wang K, Zheng W, Zhao X H, Chen Z B, Chen C Y and Yan J 2019 *J. Quant. Spectrosc. Radiat. Transf.* **236** 106586
[61] Si R, Li S, Guo X L, Chen Z B, Brage T, Jönsson P, Wang K, Yan J, Chen C Y and Zou Y M 2016 *Astrophys. J. Supp. Ser.* **227** 16
[62] Li J Q, Zhang C Y, Si R, Wang K and Chen C Y 2019 *At. Data Nucl. Data Tables* **126** 158
[63] Zhang C Y, Si R, Yao K, Gu M F, Wang K and Chen C Y 2018 *J. Quant. Spectrosc. Radiat. Transf.* **206** 180
[64] Wang K, Chen Z B, Si R, Jönsson P, Ekman J, Guo X L, Li S, Long F Y, Dang W, Zhao X H, Hutton R, Chen C Y, Yan J and Yang X 2016 *Astrophys. J. Supp. Ser.* **226** 14
[65] Kramida A, Ralchenko Y, Reader J and NIST ASD Team 2018 NIST Atomic Spectra Database (ver. 5.5.3), [Online]. Available: https://physics.nist.gov/asd [2018, March 27]. National Institute of Standards and Technology, Gaithersburg, MD.
[66] Fan Q, Jiang G, Cao L, Wang W and Du S 2013 *Eur. Phys. J. D* **67** 255
[67] Bhatia A, Landi E and Mason H 2003 *At. Data Nucl. Data Tables* **83** 71
[68] Aggarwal S, Verma N, Singh A, Singh N, Sharma R and Mohan M 2014 *Can. J. Phys.* **92** 1285
[69] Harrison R A, Sawyer E C, Carter M K, *et al.* 1995 *Sol. Phys.* **162** 233
[70] Hawryluk R, Campbell D, Janeschitz G, *et al.* 2007 *Sol. Phys.* **243** 19
[71] Watanabe T, Hara H, Yamamoto N, Kato D, Sakaue H A, Murakami I, Kato T, Nakamura N and Young P R 2009 *Astrophys. J* **692** 1294
[72] Young P R, Watanabe T, Hara H and Mariska J T 2009 *Astron. & Astrophys.* **495** 587
[73] Del Zanna G 2011 *Astron. & Astrophys.* **533** A12
[74] Yu X, Zanna G D, Stenning D C, Cisewski-Kehe J, Kashyap V L, Stein N, van Dyk D A, Warren H P and Weber M A 2018 *Astrophys. J* **866** 146
[75] Fawcett B C, Cowan R D and Hayes R W 1972 *J. Phys. B: At., Mol. Opt. Phys.* **5** 2143
[76] Fawcett B C, Cowan R D, Kononov E Y and Hayes R W 1972 *J. Phys. B: At., Mol. Opt. Phys.* **5** 1255
[77] Behring W E, Cohen L and Feldman U 1972 *Astrophys. J* **175** 493
[78] Woods T, Eparvier F, Hock R, Jones A, Woodraska D, Judge D, Didkovsky L, Lean J, Mariska J, Warren H, McMullin D, Chamberlin P, Berthiaume G, Bailey S, Fuller-Rowell T, Sojka J, Tobiska W and Viereck R 2012 *Sol. Phys.* **275** 115
[79] Woods T, Eparvier F, Hock R, Jones A, Woodraska D, Judge D, Didkovsky L, Lean J, Mariska J, Warren H, McMullin D, Chamberlin P, Berthiaume G, Bailey S, Fuller-Rowell T, Sojka J, Tobiska W and Viereck R 2012 *Sol. Phys.* **275** 115
[80] Zhang X H, Zanna G D, Wang K, Rynkun P, Jönsson P, Godefroid M, Gaigalas G, Radžiūtė L, Ma L H, Si R, Xiao J, Chen Z B, Yan J, Wu Y and Chen C Y 2021 *Astrophys. J. Supp. Ser.* **257** 56
[81] Song C X, Wang K, Del Zanna G, Jonsson P, Si R, Godefroid M, Gaigalas G, Radziute L, Rynkun P, Zhao X H, Yan J and Chen C Y 2020 *Astrophys. J. Supp. Ser.* **247** 70
[82] Wang K, Zhang X H, Zhang C Y, Dang W, Zhao X H, Chen Z B, Si R, Chen C Y and Yan J 2021 *J. Quant. Spectrosc. Radiat. Transf.* **261** 107512
[83] Wang K, Song C X, Jönsson P, Del Zanna G, Schiffmann S, Godefroid M, Gaigalas G, Zhao X H, Si R, Chen C Y and Yan J 2018 *Astrophys. J. Suppl. Ser.* **239** 30
[84] Wang K, Jönsson P, Del Zanna G, Godefroid M, Chen Z B, Chen C Y and Yan J 2020 *Astrophys. J. Suppl. Ser.* **246** 1
[85] Wang K, Jönsson P, Gaigalas G, Radžiūtė L, Rynkun P, Del Zanna G and Chen C Y 2018 *Astrophys. J. Supp. Ser.* **235** 27
[86] Del Zanna G 2012 *Astron. & Astrophys* **546** A97
[87] Del Zanna G and Storey P J 2012 *Astron. & Astrophys.* **543** A144
[88] Dufton P 1977 *Comput. Phys. Commun.* **13** 25
[89] Malinovsky L and Heroux M 1973 *Astrophys. J* **181** 1009
[90] Manson J E 1972 *Sol. Phys.* **27** 107
[91] Del Zanna G 2012 *Astron. & Astrophys.* **537** A38

[92] Behring W E, Cohen L, Doschek G A and Feldman U 1976 *Astrophys. J* **203** 521

[93] Thomas R J and Neupert W M 1994 *Astrophys. J. Supp. Ser.* **91** 461

[94] Kramida A 2013 *Fusion Sci. Technol.* **63** 313

[95] Kramida A 2014 *Astrophys. J. Supp. Ser.* **212** 11

[96] Zhang C Y, Li J Q, Wang K, Si R, Godefroid M, Jönsson P, Xiao J, Gu M F and Chen C Y 2022 *Phys. Rev. A* **105** 022817

[97] Guo X L, Huang M, Yan J, Li S, Wang K, Si R and Chen C Y 2016 *Chin. Phys. B* **25** 013101

[98] Guo X L, Li M C, Zhang C Y, Wang K, Li S, Chen Z B, Liu Y M, Zhang H J, Hutton R and Chen C Y 2018 *J. Quant. Spectrosc. Radiat. Transf.* **210** 204

[99] Wang K, Chen Z B, Chen C Y, Yan J, Dang W, Zhao X H and Yang X 2017 *At. Data Nucl. Data Tables* **117** 174

[100] Wang K, Yang X, Chen Z B, Si R, Chen C Y, Yan J, Zhao X H and Dang W 2017 *At. Data Nucl. Data Tables* **117** 1

[101] Guo X L, Grumer J, Brage T, Si R, Chen C, Jönsson P, Wang K, Yan J, Hutton R and Zou Y M 2016 *J. Phys. B: At., Mol. Opt. Phys.* **49** 135003

[102] Aggarwal K M and Keenan F P 2014 *At. Data Nucl. Data Tables* **100** 1603

[103] Aggarwal K M and Keenan F P 2016 *At. Data Nucl. Data Tables* **111–112** 187

[104] Xu M, Yan A, Wu S, Hu F and Li X 2017 *Can. J. Phys.* **95** 283

[105] Mohan M, Aggarwal S and Singh N 2014 *Can. J. Phys.* **92** 177

[106] Chen M H and Cheng K T 2011 *Phys. Rev. A* **84** 012513

[107] Quinet P 2011 *J. Phys. B: At. Mol. Opt. Phys* **44** 195007

[108] Safronova U I, Johnson W R, Kato D and Ohtani S 2001 *Phys. Rev. A* **63** 032518

[109] Safronova U I and Safronova A S 2010 *J. Phys. B: At., Mol. Opt. Phys.* **43** 074026

[110] Ding X B, Sun R, Liu J X, Koike F, Murakami I, Kato D, Sakaue H A, Nakamura N and Dong C Z 2017 *J. Phys. B: At., Mol. Opt. Phys.* **50** 045004

[111] Ding X B, Sun R, Koike F, Murakami I, Kato D, Sakaue H A, Nakamura N and Dong C Z 2018 *At. Data Nucl. Data Tables* **119** 354

[112] Ding X B, Yang J X, Koike F, Murakami I, Kato D, Sakaue H A, Nakamura N and Dong C Z 2018 *J. Quant. Spectrosc. Radiat. Transfer* **204** 7

[113] Froese Fischer C 2014 *Atoms* **2** 1

[114] Lennartsson T, Clementson J and Beiersdorfer P 2013 *Phys. Rev. A* **87** 062505

[115] Welton T A 1948 *Phys. Rev.* **74** 1157

[116] Lowe J A, Chantler C T and Grant I P 2013 *Radiat. Phys. Chem.* **85** 118

[117] Mohr P J and Kim Y K 1992 *Phys. Rev. A* **45** 2727

[118] Le Bigot E O, Indelicato P and Mohr P J 2001 *Phys. Rev. A* **64** 052508

[119] Mohr P J and Soff G 1993 *Phys. Rev. Lett.* **70** 158

[120] Beier T, Mohr P J, Persson H and Soff G 1998 *Phys. Rev. A* **58** 954

[121] Ralchenko Y, Draganic I N, Tan J N, Gillaspy J D, Pomeroy J M, Reader J, Feldman U and Holland G E 2008 *J. Phys. B: At. Mol. Opt. Phys.* **41** 021003

[122] Clementson J and Beiersdorfer P 2010 *Phys. Rev. A* **81** 052509

[123] Dyall K G, Grant I P, Johnson C T, Parpia F A and Plummer E P 1989 *Comput. Phys. Commun.* **55** 425

[124] Ekman J, Jönsson P, Radžiūtė L, Gaigalas G, Del Zanna G and Grant I P 2018 *At. Data Nucl. Data Tables* **120** 152

[125] Kramida A, Ralchenko Y, Reader J and NIST ASD Team 2020 NIST Atomic Spectra Database (ver. 5.8), [Online]. Available: https://physics.nist.gov/asd [2021, January 21]. National Institute of Standards and Technology, Gaithersburg, MD.

[126] Kramida A 2011 *Can. J. Phys.* **89** 551

[127] Cowan R D 1981 *The Theory of Atomic Structure and Spectra* (Berkeley, CA: Univ. California Press)

[128] Li Y T, Li J Q, Song C X, Zhang C Y, Si R, Wang K, Godefroid M, Gaigalas G, Jönsson P and Chen C Y 2023 *Atoms* **11** 12

[129] Li Y T, Wang K, Si R, Godefroid M, Gaigalas G, Chen C Y and Jönsson P 2023 *Comput. Phys. Commun.* **283** 108562